REVIEWS OF TOPICAL PROBLEMS

Nonlinear aspects of quantum plasma physics

Physics – Uspekhi **53** (1) 51 – 76 (2010)

REVIEWS OF TOPICAL PROBLEMS PACS numbers: 05.30.Fk, 52.35.Mw, 52.35.Ra, 52.35.Sb

Nonlinear aspects of quantum plasma physics

P K Shukla, B Eliasson

DOI: 10.3367/UFNe.0180.201001b.0055

Contents

Abstract. Dense quantum plasmas are ubiquitous in planetary interiors and in compact astrophysical objects (e.g., the interior of white dwarf stars, in magnetars, etc.), in semiconductors and micromechanical systems, as well as in the next-generation intense laser–solid density plasma interaction experiments and in quantum X-ray free-electron lasers. In contrast to classical plasmas, quantum plasmas have extremely high plasma number densities and low temperatures. Quantum plasmas are composed of electrons, positrons and holes, which are degenerate. Positrons (holes) have the same (slightly different) mass as electrons, but opposite charge. The degenerate charged particles (electrons, positrons, and holes) obey the Fermi–Dirac statistics. In quantum plasmas, there are new forces associated with (i) quantum statistical electron and positron pressures, (ii) electron and positron tunneling through the Bohm potential, and (iii) electron and positron angular momentum spin. Inclusion of these quantum forces allows the existence of very high-frequency dispersive electrostatic and electromagnetic waves (e.g., in the hard X-ray and gamma-ray regimes) with extremely short wavelengths. In this review paper, we present theoretical backgrounds for some important nonlinear aspects of wave–wave and wave–electron interactions in dense quantum plasmas. Specifically, we focus on nonlinear electrostatic electron and ion plasma waves, novel aspects of three-dimensional quantum electron fluid turbulence, as well as nonlinearly coupled intense electromagnetic waves and localized plasma wave structures. Also discussed are the phase-space kinetic structures and mechanisms that can generate quasistationary magnetic fields in dense quantum plasmas. The influence of the external magnetic field and the electron angular momentum spin on the electromagnetic wave dynamics is discussed. Finally, future perspectives of the nonlinear quantum plasma physics are highlighted.

P K Shukla Institut für Theoretische Physik IV, Fakultät für Physik und Astronomie, Ruhr–Universität Bochum,
D-44780 Bochum, Germany
Scottish Universities Physics Alliance (SUPA),
Department of Physics, University of Strathclyde, Glasgow G4 0NG, United Kingdom
Instituto de Plasmas e Fusão Nuclear, Instituto Superior Técnico, Universidade Técnica de Lisboa, 1049-001 Lisboa, Portugal
Department of Physics, Umeå University, SE-90 187 Umeå, Sweden
E-mail: profshukla@yahoo.de
B Eliasson Institut für Theoretische Physik IV, Fakultät für Physik und Astronomie, Ruhr–Universität Bochum,
D-44780 Bochum, Germany
Department of Physics, Umeå University, SE-90 187 Umeå, Sweden
Email: bengt@tp4.ruhr-uni-bochum.de

Received 19 June 2009, revised 26 August 2009
Uspekhi Fizicheskikh Nauk **180** (1) 55 – 82 (2010)
DOI: 10.3367/UFNr.0180.201001b.0055
Translated by S V Vladimirov; edited by A M Semikhatov

1. Introduction

The field of quantum plasma physics has a long and diverse tradition [1 – 5], with interest having risen recently [6, 7] connected with its potential applications in modern technology (metallic and semiconductor nanostructures such as metallic nanoparticles, metal clusters, thin metal films, spintronics, nanotubes, quantum wells and quantum dots,

nanoplasmonic devices, quantum X-ray free-electron lasers etc.). Due to the recent development of ultrafast spectroscopy techniques, it is now possible to monitor the femtosecond dynamics of an electron gas confined in metallic plasmas. In dense quantum plasmas, the number densities of degenerate electrons and/or positrons are extremely high, and the plasma particles (mainly electrons and positrons) conform to the Fermi–Dirac statistics.

The quantum degeneracy effects start playing a significant role when the de Broglie thermal wavelength $\lambda_B = \hbar/(2\pi m_e k_B T)^{1/2}$ for electrons is similar to or larger than the average inter-electron distance $n_e^{-1/3}$, i.e., when [6, 7]

$$n_e \lambda_B^3 \gtrsim 1\,, \tag{1}$$

or, equivalently, the temperature T is comparable with or lower than the electron Fermi temperature $T_{Fe} = E_F/k_B$, where the electron Fermi energy is

$$E_F = \frac{\hbar^2}{2m_e}\,(3\pi^2)^{2/3} n_e^{2/3}\,, \tag{2}$$

and hence

$$\chi = \frac{T_{Fe}}{T} = \frac{1}{2}\,(3\pi^2)^{2/3}(n_e\lambda_B^3)^{2/3} \gtrsim 1\,. \tag{3}$$

Here, $\hbar$ is the Planck constant divided by 2π, n_e is the electron number density, m_e is the rest mass of an electron, and k_B is the Boltzmann constant.

When the temperature approaches the electron Fermi temperature T_{Fe}, it can be shown using the density matrix formalism [8] that the equilibrium electron distribution function changes from the Maxwell–Boltzmann distribution $\propto \exp(-E/k_B T)$ to the Fermi–Dirac distribution

$$\propto \left(\frac{2}{\hbar^3}\right)\left[\exp\left(\frac{E-\mu}{k_B T}\right)+1\right]^{-1},$$

where E is the electron kinetic energy and μ is the chemical potential. In a dense Fermi plasma, the Thomas–Fermi screening radius is given by

$$\lambda_F = \frac{V_{Fe}}{\sqrt{3}\omega_{pe}}\,, \tag{4}$$

which is the quantum analogue of the Debye–Hückel radius. Here, the electron Fermi speed

$$V_{Fe} = \left(\frac{2E_F}{m_e}\right)^{1/2} = \frac{\hbar}{m_e}\,(3\pi^2 n_e)^{1/3} \tag{5}$$

is the speed of an electron on the Fermi surface.

A measure of the importance of collisions in a dense plasma is the quantum coupling parameter, the ratio of the interaction energy $E_{int} = e^2 n_e^{1/3}$ to the average kinetic energy E_{kin} of electrons, where e is the electron charge. For a classical plasma, the kinetic energy is $k_B T$, and hence $\Gamma_C = E_{int}/k_B T$ in the classical case. In a quantum plasma, $E_{kin} = E_F$ instead, which gives the quantum coupling parameter [6, 7, 9]

$$\Gamma_Q = \frac{E_{int}}{E_F} = \frac{2}{(3\pi^2)^{2/3}}\,\frac{m_e e^2}{\hbar^2 n_e^{1/3}} \sim \left(\frac{1}{n_e\lambda_F^3}\right)^{2/3}$$

$$\sim \left(\frac{\hbar\omega_{pe}}{2k_B T_{Fe}}\right)^2 \equiv H^2 \tag{6}$$

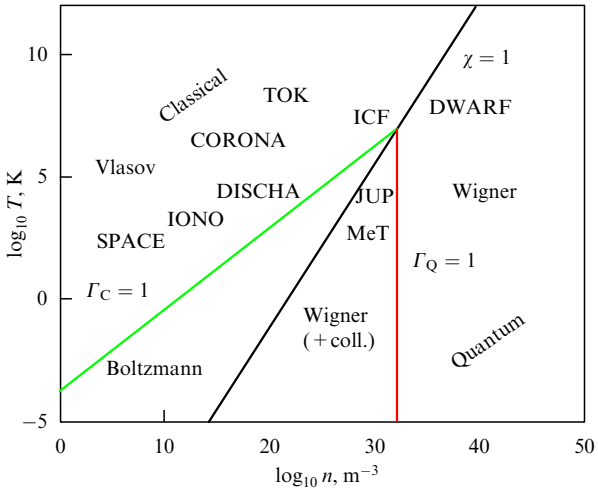

Figure 1. Schematic plasma diagram in the $\log_{10}(T)$–$\log(n)$ plane: IONO: ionospheric plasma, SPACE: space plasma, CORONA: solar corona, DISCHA: typical electric discharge, TOK: tokamak/magnetic fusion experiments, ICF: inertial confinement fusion, MET: metals and metal clusters, JUP: Jupiter's core, DWARF: white dwarf star. From Refs [6, 7].

(where we omit proportionality constants for the sake of clarity), which is analogous to the classical coupling parameter when $\lambda_F \to \lambda_D$. The various plasma regimes are illustrated in Fig. 1, where the straight lines correspond to (i) the border between the classical and quantum plasmas, $\chi = 1$, (ii) the border between collisionless and collisional classical plasmas $\Gamma_C = 1$, and (iii) the border between collisionless and collisional quantum plasmas $\Gamma_Q = 1$. In Fig. 1, various experimental and naturally occurring plasmas are exemplified and the kinetic equations used to model the plasma in each regime are indicated. The Vlasov and Wigner equations are used to respectively model collisionless plasma in the classical and quantum limits, while 'Boltzmann' indicates collisional kinetic models in a classical plasma. The kinetic models for a collisional quantum plasma are labeled 'Wigner (+coll).' We note that a quantum plasma becomes collisionless, $\Gamma_Q < 1$, when the mean distance between electrons is of the order of the Bohr radius a_0, i.e., $d = 1/n_e^{1/3} < [(3\pi^2)^{2/3}/8\pi]\,a_0 \approx 0.38 a_0$, where $a_0 = \hbar^2/m_e e^2 \approx 0.53$ Å. This corresponds to a number density of the order of $n_e \gtrsim 1.22 \times 10^{26}$ cm^{-3}, which is three orders of magnitude larger than the electron density in a typical metal; for example, $n_e = 5.9 \times 10^{22}$ cm^{-3} for gold at room temperature.

Fermi-degenerate matter demonstrates the effect called Pauli blocking, which strongly reduces the electron–electron and electron–ion collision rates. Namely, at moderate temperatures, only electrons within an energy shell with the thickness $k_B T$ near the Fermi surface (where the electron energy equals E_F) can undergo collisions. For these electrons, the electron–electron collision rate is of the order of $k_B T/\hbar$, and the average collision rate is given by this expression times T/T_F. The resulting collision frequency ν_{ee} divided by the electron plasma frequency is [7]

$$\frac{\nu_{ee}}{\omega_{pe}} \sim \frac{E_F}{\hbar\omega_p}\left(\frac{T}{T_F}\right)^2 = \frac{1}{\Gamma_Q^{1/2}}\left(\frac{T}{T_F}\right)^2. \tag{7}$$

Hence, $\nu_{ee} \ll \omega_{pe}$ when $T \ll T_F$ and $\Gamma_Q > 1$, which is relevant for metallic electrons. For example, at room temperature we

have $v_{ee} \sim 10^{11}$ s^{-1}, which is much smaller than the typical collisionless frequency of collective interactions $\omega_{pe} \sim 10^{16}$ s^{-1}. Also, the typical collision rate for electron–lattice (ion) collisions $v_{ei} \sim 10^{15}$ s^{-1} is smaller than ω_{pe} by one order of magnitude. Therefore, the collisionless regime seems to be relevant for free electrons in a metal on a time scale of the order of a femtosecond. In denser plasmas, such as in stellar interiors [10–12] and in inertial fusion schemes [13–15], the relative effects of collisions decrease even further and lead to increased electron transport and heat conductivity.

More than 60 years ago, Wigner [16] introduced a phase-space formalism to treat a quantum state of charged particles in a collisionless quantum system. He defined a quantum distribution function of phase-space variables $f(x,p,t)$ as

$$f(x,p,t)=\frac{1}{(2\pi)^{3N}}\int_{\infty}^{\infty}\rho\left(x-\frac{\hbar}{2}\,\tau,x+\frac{\hbar}{2}\,\tau,t\right)\exp\left(-\mathrm{i}p\tau\right)\mathrm{d}\tau\,, \tag{8}$$

where N is the number of particles in the system, $x\{x_1,x_2,\ldots,x_N\}$ and $p\{p_1,p_2,\ldots,p_N\}$ are the sets of coordinates and momenta for the particles, t is the time, and $\rho(x,x',t)$ is the density matrix. The Wigner function is not a probability density in phase space x, p because it can take negative values. The Wigner distribution function $W_i(x,p,t)$, corresponding to the wave function $\psi_i(x,t)$ can be expressed as

$$W_i(x,p,t)=\frac{1}{(2\pi)^{3N}\hbar}\int_{\infty}^{\infty}\mathrm{d}y\,\psi_i\left(x-\frac{y}{2},t\right)\psi_i^{*}\left(x+\frac{y}{2},t\right)\times\exp\left(-i\,\frac{py}{\hbar}\right), \tag{9}$$

and has the property

$$\int_{\infty}^{\infty}\mathrm{d}pW_i(x,p,t)=\left\langle\left|\psi_i(x,t)\right|^2\right\rangle, \tag{10}$$

where the asterisk denotes complex conjugation. The quantum kinetic equation based on the Wigner distribution was developed by Moyal [17], and is now referred to as the Wigner–Moyal description for treating statistical effects on electron plasma waves in a quantum plasma [18].

Analytic investigations of collective interactions between an ensemble of degenerate electrons in a dense quantum plasma dates back to the early 1950s. Specifically, Klimontovich and Silin [1] and Bohm and Pines [2–5] presented the properties of linear electron plasma oscillations (EPOs) in a dense quantum plasma. In such a plasma, electrons, positrons, and holes are degenerate, while ions are cold and classical (typically, the ion Fermi speed is much less than the electron Fermi speed). Accordingly, electrons, positrons, and holes have a Fermi–Dirac distribution function [19], in contrast to the Boltzmann–Maxwell distribution function for charged particles in a classical plasma.

The dispersion relation for high-frequency electron plasma oscillations in a dense quantum plasma with a fixed ion background is (see Section 10.2)

$$1-\frac{4\pi e^2}{m_e}\int\frac{f_0(\mathbf{u})}{(\omega-\mathbf{ku})^2-(\hbar^2k^4)/4m_e^2}\,\mathrm{d}^3u=0\,, \tag{11}$$

which was also obtained in [3] by performing a series of canonical transformations of the Hamiltonian of the system of individual electrons interacting via the electrostatic force. In the zero-temperature limit, we have (see Section 10.2)

$$1+\frac{3\omega_{pe}^2}{4k^2V_{Fe}^2}\left\{2-\frac{m_e}{\hbar kV_{Fe}}\left[V_{Fe}^2-\left(\frac{\omega}{k}+\frac{\hbar k}{2m_e}\right)^2\right]\times\log\left|\frac{\omega/k-V_{Fe}+\hbar k/2m_e}{\omega/k+V_{Fe}+\hbar k/2m_e}\right|+\frac{m_e}{\hbar kV_{Fe}}\times\left[V_{Fe}^2-\left(\frac{\omega}{k}-\frac{\hbar k}{2m_e}\right)^2\right]\times\log\left|\frac{\omega/k-V_{Fe}-\hbar k/2m_e}{\omega/k+V_{Fe}-\hbar k/2m_e}\right|\right\}\equiv 1+\chi_e=0\,, \tag{12}$$

which in the limit $\hbar k/m_e \to 0$ yields

$$1+\frac{3\omega_{pe}^2}{k^2V_{Fe}^2}\left(1-\frac{\omega}{2kV_{Fe}}\log\left|\frac{\omega+kV_{Fe}}{\omega-kV_{Fe}}\right|\right)=0\,, \tag{13}$$

where assume that ω is real and $\omega/k > V_{Fe}$. Here, ω is the wave frequency, $\mathbf{k}$ is the wave vector, and $\omega_{pe}=(4\pi n_e e^2/m_e)^{1/2}$ is the electron plasma frequency. On the other hand, for small wavenumbers up to terms containing k^4, it follows from (12) that

$$\omega^2\approx\omega_{pe}^2+\frac{3}{5}\,k^2V_{Fe}^2+(1+\alpha)\,\frac{\hbar^2k^4}{4m_e^2} \tag{14}$$

with $\alpha=(48/175)\,m_e^2V_{Fe}^4/\hbar^2\omega_{pe}^2\approx 2.000(a_0^3n_0)^{1/3}$, where $a_0=\hbar^2/m_ee^2\approx 53\times10^{-10}$ cm is the Bohr radius. Equation (14) shows that the wave dispersion arises due to the finite width of the electron wave function in a dense Fermi plasma [7, 20–24].

Furthermore, in the limit of low phase speed $\omega \ll kV_{Fe}$, the dielectric constant for ion oscillations becomes

$$\epsilon(\omega,\mathbf{k})\approx 1+\frac{3\omega_{pe}^2}{k^2V_{Fe}^2+3\hbar^2k^4/4m_e^2}-\frac{\omega_{pi}^2}{\omega^2}\,, \tag{15}$$

whence $\epsilon(\omega,\mathbf{k})=0$ yields the ion oscillation frequency

$$\omega\approx\frac{\omega_{pi}}{(1+Q)^{1/2}}\,, \tag{16a}$$

where $\omega_{pi}=(m_e/m_i)^{1/2}\omega_{pe}$ is the ion plasma frequency, m_i is the ion mass, $Q=3\omega_{pe}^2/(k^2V_{Fe}^2+3\hbar^2k^4/4m_e^2)$, and $\alpha \ll 1$. For $Q \gg 1$, it follows from (16a) that

$$\omega\approx kC_{Fs}\left(1+\frac{\hbar k^4}{4m_e^2\omega_{pe}^2}\right)^{1/2}, \tag{16b}$$

where $C_{Fs}=(T_{Fe}/3m_i)^{1/2}$ is the speed of sound.

Dispersion properties of electrostatic waves in an unmagnetized dense quantum plasma with arbitrary electron degeneracy have been presented in [25, 26]. The permittivity of a degenerate collisionless plasma in the random-phase approximation is given in textbooks [27, 28]. Furthermore, because a pure electromagnetic wave in a nonstreaming unmagnetized dense plasma does not accompany density fluctuations, the wave frequency is $\omega=(\omega_{pe}^2+k^2c^2)^{1/2}$, where c is the speed of light in the vacuum.The quantum statistical properties of dense plasmas in the presence of electromagnetic waves were studied theoretically in [29] and were considered in textbooks [30, 31], while quantum

parameter regimes are discussed in [6]. In a magnetized dense quantum plasma, the external magnetic field significantly affects the dynamics of degenerate electrons and positrons, and hence new collective phenomena appear associated with the electron angular momentum spin [32, 33], the electron spin magnetic moment [34], and quantized Landau energy levels [35] of fermions in a strong magnetic field. It turns out that the thermodynamics and kinetics [36] as well as the dispersion properties of both electrostatic and electromagnetic waves [37 – 43] in a quantum magnetoplasma are significantly different from those in an unmagnetized quantum plasma.

It was recognized early on that the underlying physics of nonlinear quantum-like equations can be better understood by rewriting those equations in the form of hydrodynamical (or Euler) equations, which essentially represent the evolution of quantum particle densities and momenta. This was elegantly done by Madelung [44] and Bohm [2] by introducing an eikonal representation for the wave function evolution in the nonstationary Schrödinger equation. The Madelung quantum fluid equations for the Pauli equation with the quantum particle angular momentum spin were derived in [45 – 51]. To incorporate relativistic effects into the quantum fluid formalism, the quantum electron fluid equations were derived for the Klein–Gordon equation [52] and for the Dirac equation [53 – 55]. Extensions for massless spin-1/2 particles (neutrinos) have also been added to fluid descriptions of the Weyl equation in [56].

Recently, there has been growing and vibrant interest in investigating new aspects of quantum plasma physics by developing nonrelativistic quantum hydrodynamical (QHD) equations [7, 20, 21, 57] that include the quantum statistical electron pressure and the quantum force involving tunneling of degenerate electrons through the Bohm potential [20]. The Wigner–Poisson (WP) model has also been used to derive a set of nonrelativistic QHD equations [7, 21] for a dense electron plasma under the assumption of immobile ions. The QHD equations are composed of the electron continuity, electron momentum, and Poisson equations. The quantum force [7, 20, 21] appears in the nonrelativistic electron momentum equation through the pressure term, which requires knowledge of the Wigner distribution for a quantum mixture of electron wave functions, each characterized by an occupation probability. Quantum transport models similar to the QHD plasma model have also been used in superfluidity [58] and superconductivity [59], as well as in the study of metal clusters and nanoparticles, where they are referred to as nonstationary Thomas–Fermi models [60].

The electrostatic QHD equations are useful for studying collective interactions (e.g., different types of waves, instabilities, quantum fluid turbulence, and nonlinear structures) [7, 21, 22, 61 – 69]. These give rise to high-frequency spin waves, which can be excited by neutrino beams in supernovae [40, 70 – 74]. Furthermore, studies of numerous collective interactions in dense plasmas are relevant in the context of (i) intense laser–solid density plasma experiments [13, 14, 76 – 85]; (ii) the cores of giant planets and the crusts of old stars [87 – 89]; (iii) superdense astrophysical objects [90 – 98] (e.g., interiors of white dwarfs and magnetospheres of neutron stars and magnetars); (iv) micro- and nano-scale objects (e.g., quantum diodes [99 – 104], quantum dots and nanowires [105], nanophotonics [106, 107], plasmonics [108], ultrasmall electronic devices [109 – 111], and metallic nanostructures [112]); and (v) microplasmas [113] and quantum X-ray free-electron lasers [114, 115]. Furthermore, we stress that a Fermi-degenerate dense plasma may also arise when a pellet of hydrogen is compressed to many times the solid density in the fast ignition scenario for inertial confinement fusion [15, 116, 117]. Because of the impressive development in the field of short-pulse petawatt laser technology, it is highly likely that such plasma conditions can be achieved by intense laser-pulse compression using powerful X-ray pulses. Here, ultrafast X-ray Thomson scattering techniques can be used to measure the features of laser-enhanced plasma lines, which will in turn give invaluable information regarding the equation of state of shock-compressed dense matter. Recently, spectrally resolved X-ray scattering measurements [82, 84] were performed in dense plasmas, allowing accurate measurements of the electron velocity distribution function, temperature, ionization state, and plasmons in the warm dense matter regime [118]. This novel technique promises to access the degenerate, the closely coupled, and the ideal plasma regimes, making it possible to investigate extremely dense states of matter, such as the inertial confinement fusion fuel during compression, reaching super-solid densities.

In this review, we describe the recent theoretical progress in the area of collective nonlinear interactions in collisionless dense quantum plasmas. The paper is organized as follows. In Section 2, we briefly recapitulate the hydrodynamic representation of some quantum-like models that appear in different branches of physics. The governing equations for nonlinearly interacting electrostatic waves in an unmagnetized quantum plasma are derived in Section 3. Section 4 presents numerical studies of nonlinear electron plasma wave excitations in the form of quantized one-dimensional dark solitons and quantized two-dimensional vortices. The model used here is the nonlinear Schrödinger equation for dispersive EPOs, coupled to the Poisson equation for the electrostatic potential. This model is also used for studying 3D quantum electron fluid turbulence in Section 5, where we find non-Kolmogorov-type turbulence spectra. In Section 6, we present recent results concerning the phase-space (kinetic) turbulence by using the Wigner and Vlasov models for the electron distribution function. A theoretical model for the generation of quasistationary magnetic fields in a dense quantum plasma due to the Weibel instability is presented in Section 7.1. The magnetization of a dense plasma in the presence of a large-amplitude electromagnetic wave is demonstrated in Section 7.2. The dynamics of electromagnetic waves in a dense magnetoplasma are discussed in Section 8, where we focus on spin waves propagating transversally to the magnetic field direction, and develop nonlinear equations for low-phase speed (in comparison with the speed of light) electromagnetic waves in a dense quantum magnetoplasma. Finally, Section 9 highlights our main results and describes future prospects of quantum plasma physics research.

2. Fluid representation of quantum-like models

This section is included to show how different types of quantum-like models can be reformulated in the form of hydrodynamic equations.

First, we consider the nonstationary nonlinear Schrödinger equation (NLSE)

$$\mathrm{i}\hbar\,\frac{\partial\psi}{\partial t}+\frac{\hbar^2}{2m}\,\nabla^2\psi-U_0\bigl(|\psi|^2\bigr)\,\psi=0\,, \tag{17}$$

where $\psi(\mathbf{r}, t)$ is a macroscopic wave function, m is the particle mass, and $U_0(|\psi|^2)$ is an effective potential. The NLSE also arises in various physical contexts in the description of amplitude-modulated nonlinear waves in fluids [119, 120], in transmission lines [121], in nonlinear optics for ultrafast communications [122–124], in plasmas [125–130], and in many other areas of physics [131–133].

We introduce the Madelung transformation [44]

$$\psi(\mathbf{r}, t) = \sqrt{n}\, \exp\left(\mathrm{i}\, \frac{\varphi_\mathrm{q}}{\hbar}\right), \tag{18}$$

where n and φ_q are real, and use (17) to obtain a pair of quantum hydrodynamic equations composed of the continuity and momentum equations:

$$\frac{\partial n}{\partial t} + \nabla \cdot (n\mathbf{v}) = 0\,, \tag{19}$$

and

$$m\left(\frac{\partial}{\partial t} + \mathbf{v}\cdot\nabla\right)\mathbf{v} = -\nabla\left[U_0(n) + U_\mathrm{B}\right]. \tag{20}$$

Here, $n = n(\mathbf{r}, t) = |\psi|^2$ corresponds to the local density per unit length and $\hbar\nabla\varphi_\mathrm{q}(\mathbf{r}, t) = m\mathbf{v}$. The quantum potential is

$$U_\mathrm{B} = -\frac{\hbar^2}{2m}\,\frac{\nabla^2\sqrt{n}}{\sqrt{n}}. \tag{21}$$

We note that the quantum particle number density n and the quantum velocity field $\mathbf{v}$ can be respectively written as

$$n(\mathbf{r}, t) = \psi\psi^* \equiv |\psi|^2 \tag{22}$$

and

$$\mathbf{v} = \frac{\hbar}{2\mathrm{i}m}\,\frac{(\psi^*\nabla\psi - \psi\nabla\psi^*)}{|\psi|^2} = -\frac{\mathrm{i}\hbar}{2m}\,\nabla\left[\ln\left(\frac{\psi}{\psi^*}\right)\right], \tag{23}$$

where the asterisk denotes complex conjugation. The quantum-like velocity given by (23) is a potential field, namely,

$$\nabla\times\mathbf{v} = 0 \tag{24}$$

everywhere in a singly connected region.

We now define the generalized vorticity of the weighted velocity field as [68]

$$\mathbf{\Omega} = \frac{\nabla\times\left(|\psi|^2\mathbf{v}\right)}{|\psi|^2} = \nabla\times\mathbf{v} + \frac{\nabla|\psi|^2\times\mathbf{v}}{|\psi|^2}\,, \tag{25}$$

where the first term in the right-hand side represents the ordinary vorticity. It is well known [51, 134] that in the condensate state, all the rotational flow is carried by quantized vortices (velocity circulation around the core of each such vortex is quantized). In the absence of quantized vortices, the first term is zero in view of (24). Then the second term in (25) determines the generalized vorticity. Various aspects of quantized vortex dynamics and superfluid turbulence are discussed in [134]. A technique for visualization of quantized vortices in liquid helium is presented in [135].

Second, the nonlinear Schrödinger equation can be generalized by including the trapping potential

$$V_\mathrm{b}(x, y, z) = \frac{1}{2}\, m_\mathrm{b}(\omega_x^2 x^2 + \omega_y^2 y^2 + \omega_z^2 z^2)\,, \tag{26}$$

which confines identical bosons [136] in the harmonic trap of an ultracold quantum system. Here, m_b is the boson mass and ω_x, ω_y, and ω_z are the harmonic frequencies of the bosons along the x, y, and z directions of a Cartesian coordinate system. The nonlinear dynamics of Bose–Einstein condensates (BECs) [136, 137] is then governed by the Gross–Pitaevskii equation [138–140]

$$\mathrm{i}\hbar\,\frac{\partial\phi(\mathbf{r}, t)}{\partial t} + \frac{\hbar^2}{2m}\,\nabla^2\psi(\mathbf{r}, t) - V_\mathrm{b}\psi(\mathbf{r}, t) - G|\psi|^2(\mathbf{r}, t)\,\psi(\mathbf{r}, t) = 0\,, \tag{27}$$

where $U_0(|\psi|^2) = (4\pi\hbar^2 a_\mathrm{s}/m_\mathrm{b})^{1/2}|\psi|^2 \equiv G|\psi|^2$ for the BECs. Here, m_b is the mass of the bosons and a_s is the scattering length for boson–boson collisions. The BECs are repulsive (attractive) for $G > 0$ ($G < 0$).

Introducing the ansatz $\psi(\mathbf{r}, t) = \sqrt{n_\mathrm{b}(\mathbf{r}, t)}\exp\left[\varphi_\mathrm{b}(\mathbf{r}, t)\right]$ in (27), we obtain the generalized quantum hydrodynamic equations [141, 142]

$$\frac{\partial n_\mathrm{b}}{\partial t} + \nabla\cdot(n_\mathrm{b}\mathbf{u}_\mathrm{b}) = 0 \tag{28}$$

and

$$m_\mathrm{b}\,\frac{\partial\mathbf{u}_\mathrm{b}}{\partial t} = -\nabla\left(V_\mathrm{b} + \frac{m_\mathrm{b}}{2}\,u_\mathrm{b}^2 + Gn_\mathrm{b} - \frac{\hbar^2}{2m_\mathrm{b}\sqrt{n_\mathrm{b}}}\,\nabla^2\sqrt{n_\mathrm{b}}\right), \tag{29}$$

where the particle flux is given by

$$n_\mathrm{b}(\mathbf{r}, t)\,\mathbf{u}_\mathrm{b}(\mathbf{r}, t) = \frac{\hbar^2}{2\mathrm{i}m_\mathrm{b}}\,(\psi^*\nabla\psi - \psi\nabla\psi^*) \tag{30}$$

with $\mathbf{u}_\mathrm{b} = (\hbar/m_\mathrm{b})\nabla\varphi_\mathrm{b}(\mathbf{r}, t)$. Equation (29) establishes the nonrotational nature of the superfluid motion of the BEC. Equations (29) and (30) can be used to study the linear and nonlinear properties of BECs.

Next, we consider the dynamics of a single nonrelativistic Fermi (spin 1/2) particle (a degenerate electron) governed by the Pauli equation [143, 144]

$$\mathrm{i}\hbar\,\frac{\partial\Psi}{\partial t} + \frac{\hbar^2}{2m_\mathrm{e}}\,\nabla^2\Psi - \left[\frac{\mathrm{i}e\hbar}{2m_\mathrm{e}c}\,(\mathbf{A}\cdot\nabla + \nabla\cdot\mathbf{A}) + \frac{e^2\mathbf{A}^2}{2m_\mathrm{e}c^2} - e\phi - \mu_\mathrm{e}\boldsymbol{\sigma}\cdot\mathbf{B}\right]\Psi = 0\,, \tag{31}$$

where $\Psi(\mathbf{r}, t, \boldsymbol{\sigma})$ is the wave function of the single particle species having the spin $\mathbf{s} = 1/2\boldsymbol{\sigma}$, $\boldsymbol{\sigma}$ is the Pauli spin matrices, $\mathbf{A}$ is the vector potential, ϕ is the scalar potential, $\mathbf{B} = \nabla\times\mathbf{A}$, and $\mu_\mathrm{B} = e\hbar/2m_\mathrm{e}c$ is the Bohr magneton.

With the Madelung representation for the complex wave function [145]

$$\Psi(\mathbf{r}, t, \boldsymbol{\sigma}) = s\sqrt{n_\mathrm{e}(\mathbf{r}, t, \boldsymbol{\sigma})}\,\exp\left[\frac{\mathrm{i}S_\mathrm{e}(\mathbf{r}, t, \boldsymbol{\sigma})}{\hbar}\right] \tag{32}$$

used in (31), we obtain the quantum magnetohydrodynamic equations [19, 145]

$$\frac{\partial n_\mathrm{e}}{\partial t} + \nabla\cdot\left(\frac{n_\mathrm{e}\,\mathbf{p}_\mathrm{e}}{m_\mathrm{e}}\right) = 0 \tag{33}$$

and

$$\left(\frac{\partial}{\partial t}+\frac{1}{m_\mathrm{e}}\,\mathbf{p}_\mathrm{e}\cdot\nabla\right)\mathbf{p}_\mathrm{e}=e\left[\nabla\phi+\frac{1}{c}\,\frac{\partial\mathbf{A}}{\partial t}-\frac{1}{c}\,\mathbf{v}_\mathrm{e}\times(\nabla\times\mathbf{A})\right]+\frac{\hbar^2}{2m_\mathrm{e}}\,\nabla\left(\frac{\nabla^2\sqrt{n_\mathrm{e}}}{\sqrt{n_\mathrm{e}}}\right)+\mu_\mathrm{B}\nabla(\boldsymbol{\sigma}\cdot\mathbf{B})\,, \tag{34}$$

where s mimics the spinor through which the electron spin-1/2 properties are mediated and $n_\mathrm{e}(\mathbf{r},t,\boldsymbol{\sigma})=\Psi\Psi^*$ represents the probability density of finding a single electron at some point with a spin $\mathbf{s}$. We have introduced the generalized electron momentum $\mathbf{p}_\mathrm{e}=\nabla S_\mathrm{e}-\mathrm{i}\hbar s^*\nabla s+(e/c)\,\mathbf{A}$.

We can now express the quantum electron velocity [145]

$$\mathbf{v}_\mathrm{e}=\frac{\hbar}{2m_\mathrm{e}}\,\frac{(\Psi^*\nabla\Psi-\Psi\nabla\Psi^*)}{|\Psi|^2}+\mathrm{i}\,\frac{\hbar}{m_\mathrm{e}}\,s^*\nabla s-\frac{e}{m_\mathrm{e}c}\,\mathbf{A}\,, \tag{35}$$

the spin density vector

$$\mathbf{s}=\frac{\hbar}{2}\,s^*\boldsymbol{\sigma}s\,, \tag{36}$$

and the spin vector transport equation [45]

$$\frac{\mathrm{d}\mathbf{s}}{\mathrm{d}t}=\frac{e}{m_\mathrm{e}c}\,(\mathbf{s}\times\mathbf{B})+\frac{1}{m_\mathrm{e}n_\mathrm{e}}\left[\mathbf{s}\times\frac{\partial}{\partial x_k}\left(n_\mathrm{e}\,\frac{\partial\mathbf{s}}{\partial x_k}\right)\right], \tag{37}$$

where we use the summation convention for repeated indices, and introduce the total derivative $\mathrm{d}/\mathrm{d}t\equiv(\partial/\partial t)+\mathbf{v}_\mathrm{e}\cdot\nabla$. The electron momentum and electromagnetic fields are coupled via the Maxwell equations.

Ignoring the electromagnetic fields and the particle spin, and linearizing (33) and (34), we obtain the frequency of electron oscillations

$$\omega_\mathrm{g}=\frac{\hbar k^2}{2m_\mathrm{e}}\,, \tag{38}$$

where k is the wave number.

Finally, we consider the interaction of an electron with both background electrons and singly charged positive ions. The electron dynamics are governed by [146]

$$\mathrm{i}\hbar\,\frac{\partial\psi}{\partial t}+\frac{\hbar^2}{2m_\mathrm{e}}\,\nabla^2\psi-U\big(|\psi|^2\big)=0\,, \tag{39}$$

where

$$U\big(|\psi|^2\big)=e^2\int\mathrm{d}^3\mathbf{r}'\,\frac{1}{|\mathbf{r}-\mathbf{r}'|}\Big(\big|\psi(\mathbf{r}',t)\big|^2-n_\mathrm{i}(\mathbf{r}',t)\Big) \tag{40}$$

is the potential responsible for the interaction of an electron with background matter, which includes electrons and positively charged ions with the number density $n_\mathrm{i}(\mathbf{r}',t)$.

The wave function is normalized to the number density of electrons, $n_\mathrm{e}(\mathbf{r},t)=\big|\psi(\mathbf{r},t)\big|^2$. We note that Eqn (39) accounts only for the Coulomb interactions between electrons and ions, and completely ignores the quantum statistical pressure, the self-consistent ambipolar field arising from charge separation, and the electron spin-1/2 effect.

We assume that $\psi(\mathbf{r},t)=\psi_0+\psi_1(\mathbf{r},t)$, where $|\psi_0|^2=n_0$ represents the unperturbed electron number density and the perturbation wave function $\psi_1(\mathbf{r},t)$ for spherically symmetric oscillations has the form $(A_k/r)\,\sin(kr)\exp(-\mathrm{i}\omega t)$, with A_k being a normalization constant. Then the dispersion relation deduced from (39) is [146]

$$k^2=\frac{\omega m_\mathrm{e}}{\hbar}\left[1\pm\left(1-4\,\frac{\omega_\mathrm{pe}^2}{\omega^2}\right)^{1/2}\right]. \tag{41}$$

The interaction between two electrons participating in spherically symmetric electron oscillations has been considered in Ref. [146]. This study predicts an effective attraction between electrons mediated by low-energy [with the minus sign in Eqn (41)] spherically symmetric oscillations of electrons in a quantum plasma. We can thus have attracting degenerate electrons in dense plasmas. The underlying physics of electron attraction seems to be similar to that of the Cooper pairing of electrons in superconductors in which the electrons close to the Fermi level attract each other due to their interactions with crystal lattice vibrations (phonon oscillations). The pairs of electrons act more like bosons, which can condense to the same energy level, contrarily to single electrons, which are fermions and must obey the Pauli exclusion principle.

3. Nonlinear equations for unmagnetized quantum plasmas

In the preceding section, we saw that the quantum Madelung fluid description predicts a diffraction pattern of a single electron or positron. However, collective interactions between an ensemble of degenerate electrons (fermions) in dense plasmas are responsible for new linear and nonlinear waves and structures.

The quantum N-body problem is governed by the Schrödinger equation for the N-particle wave function $\psi(q_1,q_2,\ldots,q_N,t)$, where $q_j=(\mathbf{r}_j,s_j)$ is the coordinate (space, spin) of particle j. For identical fermions, the equilibrium N-particle wave function is given by the Slater determinant [8]

$$\psi(q_1,\,q_2,\,\ldots,\,q_N,t)=\frac{1}{\sqrt{N!}}\begin{vmatrix}\psi_1(q_1,t) & \psi_2(q_1,t) & \cdots & \psi_N(q_1,t)\\ \psi_1(q_2,t) & \psi_2(q_2,t) & \cdots & \psi_N(q_2,t)\\ \vdots & \vdots & \ddots & \vdots\\ \psi_1(q_N,t) & \psi_2(q_N,t) & \cdots & \psi_N(q_N,t)\end{vmatrix}, \tag{42}$$

which is antisymmetric under odd permutations. Hence, ψ vanishes if two rows are identical, which is an expression of the Pauli exclusion principle that two identical fermions cannot occupy the same state. For example $(N=2)$,

$$\psi(q_1,q_2,t)=\frac{1}{\sqrt{2}}\left[\psi_1(q_1,t)\,\psi_2(q_2,t)-\psi_1(q_2,t)\,\psi_2(q_1,t)\right],$$

and hence $\psi(q_2,q_1,t)=-\psi(q_1,q_2,t)$ and $\psi(q_1,q_1,t)=0$. Due to the Pauli exclusion principle, all electrons together are not permitted to occupy the lowest energy state, and in the ultra-cold limit, when all energy states up to the Fermi energy level are occupied by electrons, there is still a quantum-statistical pressure determined by the Fermi pressure.

In describing collective electrostatic oscillations in a plasma, the quantum analogue of the Vlasov–Poisson system is the Wigner–Poisson system given by

$$\frac{\partial f}{\partial t}+\mathbf{v}\cdot\nabla f=-\frac{\mathrm{i}em_\mathrm{e}^3}{(2\pi)^3\hbar^4}\iint\exp\left[\mathrm{i}m_\mathrm{e}(\mathbf{v}-\mathbf{v}')\,\frac{\boldsymbol{\lambda}}{\hbar}\right]\times\left[\phi\left(\mathbf{x}+\frac{\boldsymbol{\lambda}}{2},t\right)-\phi\left(\mathbf{x}-\frac{\boldsymbol{\lambda}}{2},t\right)\right]f(\mathbf{x},\mathbf{v}',t)\;\mathrm{d}^3\lambda\;\mathrm{d}^3v'\,, \tag{43}$$

and

$$\nabla^2\phi = 4\pi e\left(\int f\,\mathrm{d}^3v - n_0\right), \tag{44}$$

under the assumption of immobile ions. We note (see Section 10.1) that the Wigner equation tends to the Vlasov equation for classical particles (electrons), i.e., as $\hbar \to 0$:

$$\frac{\partial f}{\partial t} + \mathbf{v}\cdot\nabla f = -\frac{e}{m_\mathrm{e}}\nabla\phi\cdot\frac{\partial f}{\partial \mathbf{v}}\,. \tag{45}$$

We now take the moments of Wigner equation (43) and obtain [up to $O(\hbar^2)$] the equations for a nonrelativistic quantum-electron fluid (or the quantum Madelung fluid) [7, 21], specifically, the electron continuity equation

$$\frac{\partial n_\mathrm{e}}{\partial t} + \nabla\cdot(n_\mathrm{e}\mathbf{u}_\mathrm{e}) = 0 \tag{46}$$

and the electron momentum equation involving the quantum statistical pressure and the quantum force

$$m_\mathrm{e}\left(\frac{\partial}{\partial t} + \mathbf{u}_\mathrm{e}\cdot\nabla\right)\mathbf{u}_\mathrm{e} = e\nabla\phi - \frac{1}{n_\mathrm{e}}\nabla P_\mathrm{e} + \mathbf{F}_Q\,, \tag{47}$$

where ϕ is determined from the Poisson equation

$$\nabla^2\phi = 4\pi e(n_\mathrm{e} - n_0)\,. \tag{48}$$

For the degenerate Fermi–Dirac-distributed plasma (up to constants of the order of unity), the quantum statistical pressure for the electrons applies:

$$P_\mathrm{e} = \frac{m_\mathrm{e}V_\mathrm{Fe}^2 n_0}{3}\left(\frac{n_\mathrm{e}}{n_0}\right)^{(D+2)/D}, \tag{49}$$

where D is the number of degrees of freedom in the system. We note that different expressions for P_e in the nonzero limit of the electron Fermi temperature were obtained in [69] and [19].

The quantum force [20] due to electron tunneling through the Bohm potential is

$$\mathbf{F}_\mathrm{Q} = \frac{\hbar^2}{2m_\mathrm{e}}\nabla\left(\frac{\nabla^2\sqrt{n_\mathrm{e}}}{\sqrt{n_\mathrm{e}}}\right) \equiv -\nabla\phi_\mathrm{B}\,, \tag{50}$$

where ϕ_B represents the Bohm potential. We note that the α-term [cf. (14)] does not appear in (50) due to consideration of terms up to $O(\hbar^2)$ in the expansion parameter, as is also the case when the mean-field approximation [20] is used in deriving $\mathbf{F}_\mathrm{Q}$.

3.1 Nonlinear Schrödinger–Poisson equations

With the wave function introduced as

$$\psi(\mathbf{r},t) = \sqrt{n_\mathrm{e}(\mathbf{r},t)}\exp\left(\mathrm{i}\,\frac{\varphi_\mathrm{e}(\mathbf{r},t)}{\hbar}\right), \tag{51}$$

where S is defined according to $m_\mathrm{e}\mathbf{u}_\mathrm{e} = \nabla\varphi_\mathrm{e}$ and $n_\mathrm{e} = |\psi|^2$, it can be shown that the QHD equations [e.g., Eqns (46)–(48)] are equivalent to the generalized NLS–Poisson system [7, 21]

$$\mathrm{i}\hbar\frac{\partial\psi}{\partial t} + \frac{\hbar^2}{2m_\mathrm{e}}\nabla^2\psi + e\phi\psi - \frac{m_\mathrm{e}V_\mathrm{Fe}^2}{2n_0^2}|\psi|^{4/D}\psi = 0 \tag{52}$$

and

$$\nabla^2\phi = 4\pi e\left(|\psi^2| - n_0\right). \tag{53}$$

The derivation of (52) requires the electron plasma flow velocity to be curl-free everywhere in a singly connected region, except at points where the electron number density vanishes. This is obviously not valid in general. Similarly to the quantum-fluid treatment, we should include the generalized electron vorticity $\boldsymbol{\Omega}_\mathrm{e} = \nabla\times(|\psi|^2\mathbf{u}_\mathrm{e})/|\psi|^2$, which is nonvanishing [see the discussions below Eqn (25)]. Equation (52) captures the two main properties of a quantum plasma, the quantum statistical pressure (fully nonlinear) and quantum dispersion effects, and is self-consistently coupled to the electrostatic potential via Poisson equation (53). We thus have a nonlocal nonlinear interaction between the electron density and the electrostatic potential. Furthermore, we note that the one-dimensional version of Eqn (52) without the ϕ term has also been used to describe the behavior of a BEC [147] in the absence of the confining potential.

Linearization of the NLS–Poisson equations yields the frequency of the EPOs [1, 2, 4, 5]:

$$\omega_k = \left(\omega_\mathrm{pe}^2 + k^2V_\mathrm{Fe}^2 + \frac{\hbar^2k^4}{4m_\mathrm{e}^2}\right)^{1/2}. \tag{54}$$

Two distinct dispersive effects follow from (54): the long-wavelength regime $V_\mathrm{Fe} \gg \hbar k/2m_\mathrm{e}$ and the short-wavelength regime $V_\mathrm{Fe} \lesssim \hbar k/2m_\mathrm{e}$, separated by the critical wavenumber $k_\mathrm{cr} = 2\pi/\lambda_\mathrm{cr} = \pi\hbar/m_\mathrm{e}V_\mathrm{Fe} \sim n_\mathrm{e}^{-1/3}$.

3.2 Inclusion of ion dynamics

The dynamics of low phase speed (in comparison with the electron Fermi speed) nonlinear electrostatic ion oscillations in a quantum electron–ion plasma are governed by the inertialess electron equation of motion

$$0 = e\nabla\phi - \frac{1}{n_\mathrm{e}}\nabla P_\mathrm{e} + \mathbf{F}_Q\,, \tag{55}$$

the ion continuity equation

$$\frac{\partial n_\mathrm{i}}{\partial t} + \nabla\cdot(n_\mathrm{i}\mathbf{u}_\mathrm{i}) = 0\,, \tag{56}$$

the ion momentum equation

$$m_\mathrm{i}n_\mathrm{i}\left(\frac{\partial}{\partial t} + \mathbf{u}_\mathrm{i}\cdot\nabla\right)\mathbf{u}_\mathrm{i} = -Z_\mathrm{i}n_\mathrm{i}e\nabla\phi\,, \tag{57}$$

and the Poisson equation

$$\nabla^2\phi = 4\pi e(n_\mathrm{e} - Z_\mathrm{i}n_\mathrm{i})\,, \tag{58}$$

where n_i is the ion number density, $\mathbf{u}_\mathrm{i}$ is the ion fluid velocity, and Z_i is the ion charge state.

In the quasineutral approximation $n_\mathrm{i} = Z_\mathrm{i}n_\mathrm{i} = n$, we can combine Eqns (55) and (57) to obtain

$$\left(\frac{\partial}{\partial t} + \mathbf{u}_\mathrm{i}\cdot\nabla\right)\mathbf{u}_\mathrm{i} = -\frac{C_\mathrm{Fs}^2n_0}{n_\mathrm{i}}\nabla\left(\frac{Z_\mathrm{i}n_\mathrm{i}}{n_0}\right)^{(D+2)/D} + \frac{\hbar^2}{2m_\mathrm{e}m_\mathrm{i}}\nabla\left(\frac{\nabla^2\sqrt{Z_\mathrm{i}n_\mathrm{i}}}{\sqrt{Z_\mathrm{i}n_\mathrm{i}}}\right). \tag{59}$$

Equations (56) and (59) are the desired set for studying nonlinear ion waves [61, 62] in a dense quantum plasma.

4. Localized electrostatic excitations

We are now in a position to discuss nonlinear properties and the dynamics of localized electrostatic excitations in a dense quantum plasma based on the nonlinear equations derived in the preceding section.

4.1 Dark solitons and vortices associated with EPOs

In this subsection, we discuss the formation of one-dimensional quantized dark solitons and two-dimensional (2D) quantized vortices associated with the EPOs in a dense quantum plasma at nanoscales (of the order of $V_{\rm Fe}/\omega_{\rm pe}$). We note that the dynamics of dark solitons in the 2D nonlinear Schrödinger equation in a defocusing medium have been studied in [148, 149]. However, for studying the formation and dynamics of electrostatic nanostructures in a dense quantum plasma, we use the nonlinear Schrödinger–Poisson equations [22]

$$\mathrm{i}\,\frac{\partial \Psi}{\partial t} + A\nabla^2\Psi + \varphi\Psi - |\Psi|^{4/D}\Psi = 0 \tag{60}$$

and

$$\nabla^2\varphi = |\Psi|^2 - 1\,, \tag{61}$$

where the normalized wave function Ψ is $\psi/\sqrt{n_0}$, the normalized φ is $e\phi/k_{\rm B}T_{\rm Fe}$, and the time and space variables are respectively expressed in units of $V_{\rm Fe}/\omega_{\rm pe}$ and $\hbar/k_{\rm B}T_{\rm Fe}$. We set $A = 4\pi m_{\rm e}e^2/\hbar^2 n_0^{1/3}$ (see Ref. [22]).

System of equations (60) and (61) is supplemented by the Maxwell equation

$$\frac{\partial \mathbf{E}}{\partial t} = \mathrm{i}A\left(\Psi\nabla\Psi^* - \Psi^*\nabla\Psi\right), \tag{62}$$

where the electric field is $\mathbf{E} = -\nabla\phi$.

System (60)–(62) has the following conserved integrals: the number of electrons

$$N = \int |\Psi|\,\mathrm{d}^3x\,, \tag{63}$$

the electron momentum

$$\mathbf{P} = -\mathrm{i}\int \Psi^*\nabla\Psi\,\mathrm{d}^3x\,, \tag{64}$$

the electron angular momentum

$$\mathbf{L} = -\mathrm{i}\int \Psi^*\mathbf{r}\times\nabla\Psi\,\mathrm{d}^3x\,, \tag{65}$$

and the total energy

$$\mathcal{E} = \int\left[-\Psi^*A\nabla^2\Psi + \frac{|\nabla\varphi|^2}{2} + \frac{|\Psi|^{2+4/D}D}{2+D}\right]\mathrm{d}^3x\,. \tag{66}$$

The conserved quantities are required to check the accuracy of numerical integration of (60) and (61).

For quasistationary one-dimensional structures moving with a constant speed v_0, localized, solitary wave solutions can be found by introducing the ansatz $\Psi = W(\xi)\times\exp(\mathrm{i}Kx - \mathrm{i}\Omega t)$, where W is a complex-valued function of $\xi = x - v_0t$, and K and Ω are a constant wavenumber and the frequency shift. With the choice $K = v_0/2A$, the coupled system of equations can be written as

$$\frac{\mathrm{d}^2W}{\mathrm{d}\xi^2} + \lambda W + \frac{\varphi W}{A} - \frac{|W|^4W}{A} = 0 \tag{67}$$

and

$$\frac{\mathrm{d}^2\varphi}{\mathrm{d}\xi^2} = |W|^2 - 1\,, \tag{68}$$

where $\lambda = \Omega/A - v_0^2/4A^2$ is an eigenvalue of the system. From the boundary conditions $|W| = 1$ and $\varphi = 0$ at $|\xi| = \infty$, we determine $\lambda = 1/A$ and $\Omega = 1 + v_0^2/4A$. System of equations (67) and (68) admits a first integral in the form

$$\mathcal{H} = A\left|\frac{\mathrm{d}W}{\mathrm{d}\xi}\right|^2 - \frac{1}{2}\left(\frac{\mathrm{d}\varphi}{\mathrm{d}\xi}\right)^2 + |W|^2 - \frac{|W|^6}{3} + \varphi|W|^2 - \varphi - \frac{2}{3} = 0\,, \tag{69}$$

where the boundary conditions $|W| = 1$ and $\varphi = 0$ at $|\xi| = \infty$ have been used.

Figure 2 shows the profiles of $|W|^2$ and φ obtained numerically from (67) and (68) for several values of A, where W was set to -1 on the left boundary and to $+1$ on the right boundary, i.e., the phase shift is 180 degrees between the two boundaries. The solutions are in the form of dark solitons, with a localized depletion of the electron density $N_{\rm e} = |W|^2$ associated with a localized positive potential. Larger values of the quantum coupling parameter A give rise to larger-amplitude and wider dark solitons. The solitons exhibit localized 'shoulders' on both sides of the density depletion.

Numerical solutions of the time-dependent system of Eqns (60) and (61) are displayed in Fig. 3, with initial conditions close (but not equal) to the ones in Fig. 2. Two

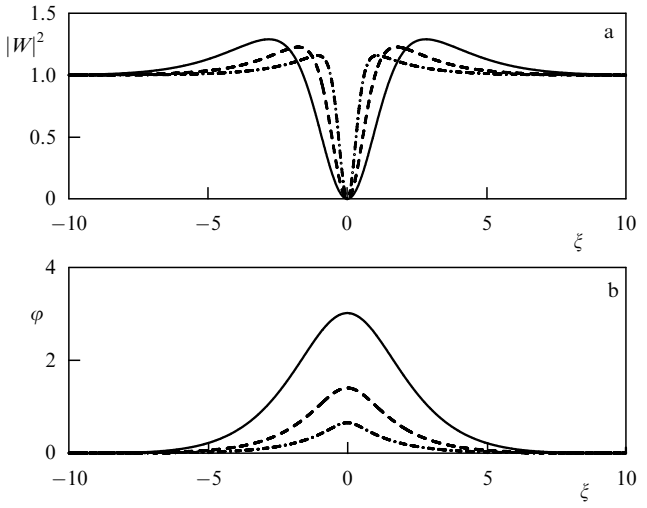

Figure 2. The electron density $|W|^2$ (upper panel) and electrostatic potential φ (lower panel) associated with a dark soliton supported by system of equations (67) and (68) for $A = 5$ (solid lines), $A = 1$ (dashed lines), and $A = 0.2$ (dashed-dotted line). From Ref. [22].

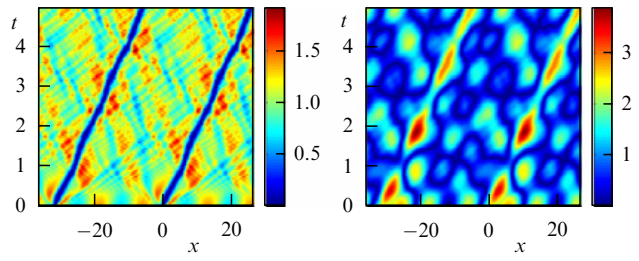

Figure 3. The time development of the electron density $|W|^2$ (left panel) and electrostatic potential φ (right panel) obtained from a simulation of system of equations (60) and (61). The initial condition is $\Psi = 0.18 + \tanh[20\sin(x/10)]\exp(\mathrm{i}Kx)$, with $K = v_0/2A$, $A = 5$, and $v_0 = 5$. From Ref. [22].

very clear and long-lived dark solitons are visible, associated with a positive potential $\varphi \approx 3$, in agreement with the quasistationary solution of Fig. 2 for $A = 5$. In addition, there are oscillations and wave turbulence in the time-dependent solution presented in Fig. 3. Hence, the dark solitons seem to be robust structures that can withstand perturbations and turbulence for a considerable time.

For the 2D system, it is possible to find vortex structures of the form $\Psi = \psi(r)\exp(\mathrm{i}s\theta - \mathrm{i}\Omega t)$, where r and θ are the polar coordinates defined via $x = r\cos(\theta)$ and $y = r\sin(\theta)$, Ω is a constant frequency shift, and $s = 0, \pm 1, \pm 2, \ldots$ for different excited states (charge states). The index s is also known as the circulation number [51]. With this ansatz, Eqns (60) and (61) can be respectively written as

$$\left[\Omega + A\left(\frac{\mathrm{d}^2}{\mathrm{d}r^2} + \frac{1}{r}\frac{\mathrm{d}}{\mathrm{d}r} - \frac{s^2}{r^2}\right) + \varphi - |\psi|^2\right]\psi = 0 \qquad (70)$$

and

$$\left(\frac{\mathrm{d}^2}{\mathrm{d}r^2} + \frac{1}{r}\frac{\mathrm{d}}{\mathrm{d}r}\right)\varphi = |\psi|^2 - 1\,, \qquad (71)$$

where the boundary conditions $\psi = 1$ and $\varphi = \mathrm{d}\psi/\mathrm{d}r = 0$ at $r = \infty$ determine the constant frequency $\Omega = 1$. Different signs of charge state s describe different rotation directions of the vortex. For $s \neq 0$, we must have $\psi = 0$ at $r = 0$, and from symmetry considerations, we have $\mathrm{d}\varphi/\mathrm{d}r = 0$ at $r = 0$. Figure 4 shows numerical solutions of Eqns (70) and (71) for different s and for $A = 5$. Here, the vortex is characterized by a complete depletion of the electron density at the core of the vortex, and is associated with a positive electrostatic potential.

Figure 5 shows time-dependent solutions of Eqns (60) and (61) in two spatial dimensions for singly charged ($s = \pm 1$) vortices with the initial condition given by four vortex-like structures placed at some distance from each other. The initial conditions were such that the vortices were organized into two vortex pairs, with $s_1 = +1$, $s_2 = -1$, $s_3 = -1$, and $s_4 = +1$, seen in the upper panels of Fig. 5. The vortices in the pairs have the opposite polarity of the electron fluid rotation, as seen in the upper right panel in Fig. 5. Interestingly, the 'partners' in the vortex pairs attract each other and propagate together with a constant velocity, and in the collision and interaction of the vortex pairs (see the second and third pairs of panels in Fig. 5), the vortices preserve their identities and change partners, resulting in two new vortex pairs that propagate obliquely to the original propagation direction. On the other hand, as shown in Fig. 6, vortices that are multiply charged ($|s_j| > 1$) are unstable. Here, system of

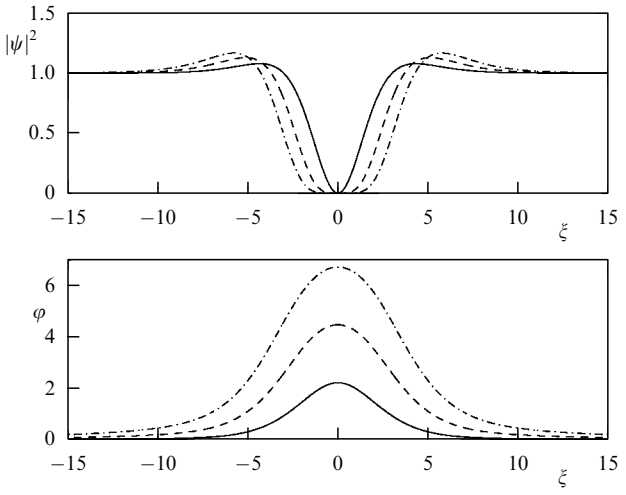

Figure 4. The electron density $|\psi|^2$ (upper panel) and electrostatic potential φ (lower panel) associated with a two-dimensional vortex supported by system (70) and (71), for the charge states $s = 1$ (solid lines), $s = 2$ (dashed lines) and $s = 3$ (dashed-dotted lines). We used $A = 5$ in all cases. From Ref. [22].

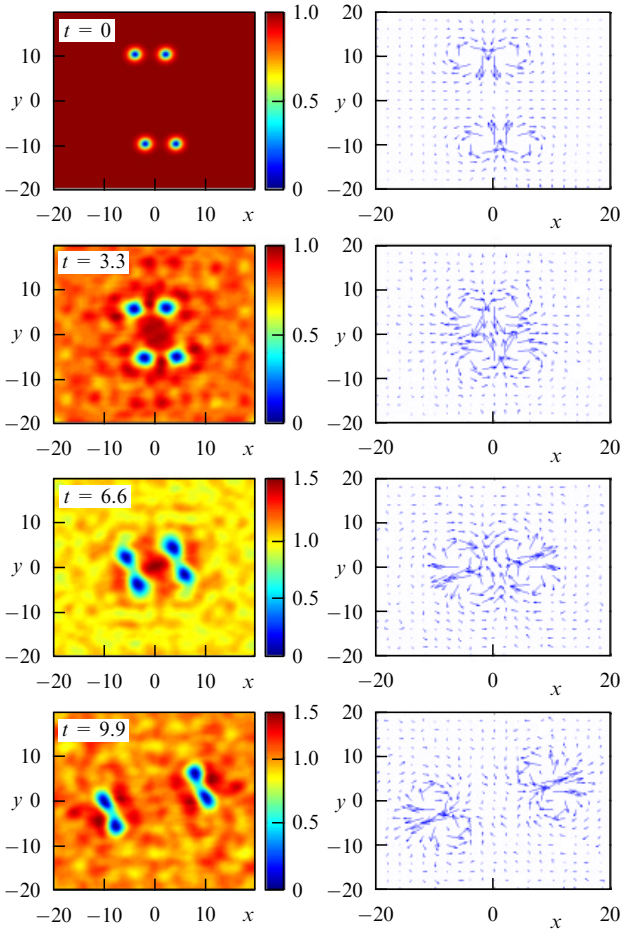

Figure 5. The electron density $|\Psi|^2$ (left panel) and an arrow plot of the electron current $\mathrm{i}(\Psi\nabla\Psi^* - \Psi^*\nabla\Psi)$ (right panel) associated with singly charged ($|s| = 1$) two-dimensional vortices, obtained from a simulation of the time-dependent system of equations (60) and (61) at times $t = 0$, $t = 3.3$, $t = 6.6$, and $t = 9.9$ (from top down). We used $A = 5$. The singly charged vortices form pairs and preserve their identities. From Ref. [22].

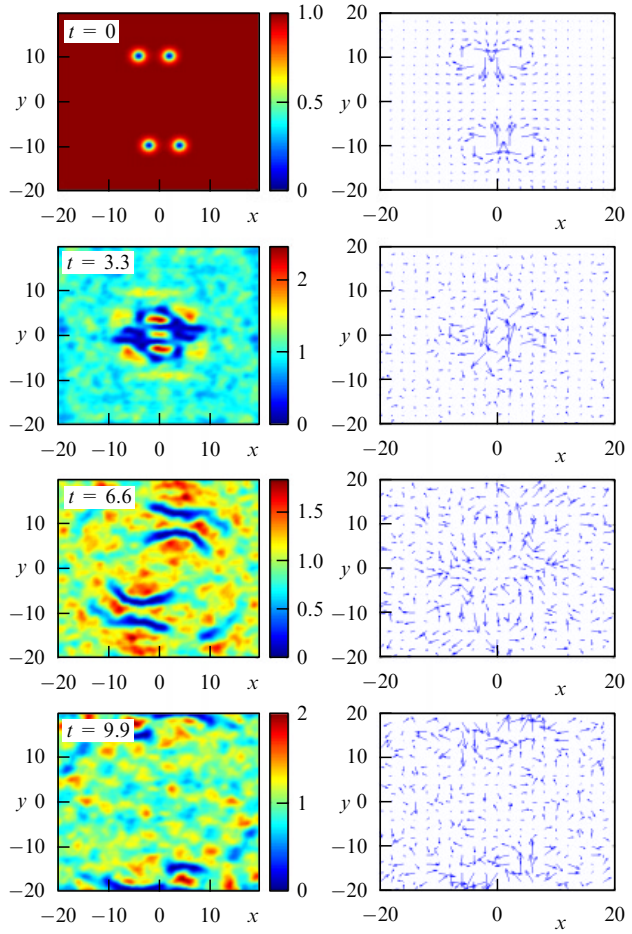

Figure 6. The electron density $|\Psi|^2$ (left panel) and an arrow plot of the electron current $\mathrm{i}(\Psi\nabla\Psi^* - \Psi^*\nabla\Psi)$ (right panel) associated with double charged ($|s| = 2$) two-dimensional vortices, obtained from a simulation of the time-dependent system of Eqns (60) and (61) at times $t = 0$, $t = 3.3$, $t = 6.6$, and $t = 9.9$ (from top down). We used $A = 5$. The doubly charged vortices dissolve into nonlinear structures and wave turbulence. From Ref. [22].

equations (60) and (61) was again solved numerically with the same initial condition as the one in Fig. 5, but with doubly charged vortices $s_1 = +2$, $s_2 = -2$, $s_3 = -2$, and $s_4 = +2$. The second row of panels in Fig. 6 reveals that the vortex pairs preserve their identities for some time, while a quasi one-dimensional density cavity is formed between the two vortex pairs. At a later stage, the four vortices dissolve into complicated nonlinear structures and wave turbulence. Hence, the nonlinear dynamics are very different between singly and multiply charged solitons, where only singly charged vortices are long-lived and keep their identities. This is in line with previous results for the nonlinear Schrödinger equation, where it was noted that vortices with higher charge states are unstable [249].

4.2 Localized ion wave excitations in quantum plasmas

In their classic paper, Haas et al. [61] developed both small- and large-amplitude theories for one-dimensional solitary ion waves in a dense quantum plasma. They found that the dynamics of small-amplitude solitary waves are governed by the Korteweg–de Vries (KdV) equation

$$\frac{\partial U}{\partial \tau} + 2U\frac{\partial U}{\partial \xi} + \frac{1}{2}\left(1 - \frac{H}{8}\right)\frac{\partial^3 U}{\partial \xi^3} = 0\,, \tag{72}$$

where U represents the relative (with respect to n_0) ion density perturbation and the time and space variables are respectively expressed in units of the ion plasma period $\omega_{\mathrm{pi}}^{-1}$ and the Thomas–Fermi electron radius $(k_{\mathrm{B}}T_{\mathrm{Fe}}/4\pi n_0 e^2)^{1/2}$.

The KdV equation allows both solitary and periodic (cnoidal) waves [150]. Introducing the wave form $U(\eta = \xi - M_{\mathrm{s}}\tau)$, we can write (72) in the stationary frame as

$$\frac{1}{2}\left(1 - \frac{H}{8}\right)\frac{\partial^2 U}{\partial \eta^2} - M_{\mathrm{s}}U + U^2 + C = 0\,, \tag{73}$$

where M_{s} is the Mach number and C is a constant of integration. In the special case where U and its derivatives tend to zero at $\pm\infty$, $C = 0$. Multiplying (73) by $\partial U/\partial\eta$, we can integrate the resultant equation once, and express it in the form of an energy integral [151 – 153]. The resulting solitary wave solution of (73) is

$$U = U_{\mathrm{m}}\,\mathrm{sech}^2\left(\frac{\eta}{\eta_0}\right), \tag{74}$$

where $U_{\mathrm{m}} = (3M_{\mathrm{s}}/2)$ and $\eta_0 = (2/M_{\mathrm{s}})^{1/2}(1 - H/8)^{1/2}$ are the maximum amplitude and the width of the soliton. We see that compressive solitary wave solutions are possible if $0 < H < 8$.

One-dimensional large-amplitude localized ion wave excitations are also possible. To demonstrate this, we assume that the quantum force acting on the electrons dominates over the quantum statistical pressure, $k_{\mathrm{B}}T_{\mathrm{Fe}}n_{\mathrm{e}} \ll (\hbar^2/4m_{\mathrm{e}})\,\partial^2 n_{\mathrm{e}}/\partial x^2$. Hence, the electron density is obtained from [62]

$$e\phi + \frac{\hbar^2}{2m_{\mathrm{e}}\sqrt{n_{\mathrm{e}}}}\frac{\partial^2\sqrt{n_{\mathrm{e}}}}{\partial x^2} = 0\,. \tag{75}$$

The electrons are coupled to ions through the space charge electric field $(-\nabla\phi)$.

The dynamics of singly charged ions are governed by the ion continuity

$$\frac{\partial n_{\mathrm{i}}}{\partial t} + \frac{\partial (n_{\mathrm{i}}u_{\mathrm{i}})}{\partial x} = 0\,, \tag{76}$$

and ion momentum equation

$$m_{\mathrm{i}}\left(\frac{\partial}{\partial t} + u_{\mathrm{i}}\frac{\partial}{\partial x}\right)u_{\mathrm{i}} = -e\frac{\partial\phi}{\partial x}\,, \tag{77}$$

where u_{i} is the x component of the ion fluid velocity perturbation. System of equations (75)–(77) is closed by the Poisson equation

$$\frac{\partial^2\phi}{\partial x^2} = 4\pi e(n_{\mathrm{e}} - n_{\mathrm{i}})\,. \tag{78}$$

We now seek stationary nonlinear ion wave structures moving with a constant speed u_0. Hence, all unknowns depend on only the variable $\xi = x - u_0 t$. With $\sqrt{n_{\mathrm{e}}} \equiv \psi$, Eqn (75) takes the form

$$\frac{\hbar^2}{2m_{\mathrm{e}}}\frac{\partial^2\psi}{\partial\xi^2} + e\phi\psi = 0\,. \tag{79}$$

Equations (76) and (77) can be integrated once with the boundary conditions $n_{\mathrm{i}} = n_0$ and $u_{\mathrm{i}} = 0$ at $\xi = |\infty|$, and the

results can be combined to yield

$$n_i = \frac{n_0 u_0}{\sqrt{u_0^2 - 2e\phi/m_i}} \,. \tag{80}$$

Substituting (80) in (78), we obtain

$$\frac{\partial^2 \phi}{\partial \xi^2} = 4\pi e\left(\psi^2 - \frac{n_0 u_0}{\sqrt{u_0^2 - 2e\phi/m_i}}\right). \tag{81}$$

Equations (79) and (81) are the desired equations for studying nonlinear ion waves in dense quantum plasmas.

It is convenient to introduce dimensionless quantities in Eqns (79) and (81), and rewrite them as

$$\frac{\partial^2 \Psi}{\partial X^2} + \frac{\Phi \Psi}{2} = 0 \tag{82}$$

and

$$\frac{\partial^2 \Phi}{\partial X^2} - \Psi^2 + \frac{M}{\sqrt{M - 2\Phi}} = 0 \,, \tag{83}$$

where we have normalized the space variable as $X = k_q \xi$, the electron wave function as $\Psi = \sqrt{n_0}\psi$, and the potential as $\Phi = e\phi/m_i c_q^2$. Here, $c_q = \omega_{pi}/k_q$ is the quantum ion wave speed and $k_q = (2m_e\omega_{pe}/\hbar)^{1/2}$ is the quantum wavenumber. The quantum 'Mach number' is defined as $M = u_0/c_q$.

We note that the coupled equations (82) and (83) admit the conserved quantity

$$\mathcal{H} = -2\left(\frac{\partial \Psi}{\partial X}\right)^2 + \frac{1}{2}\left(\frac{\partial \Phi}{\partial X}\right)^2 - \Phi\Psi^2 - M\left(\sqrt{M^2 - 2\Phi} - M\right) = 0 \,, \tag{84}$$

where we use the boundary conditions $\Phi = \partial\Phi/\partial X = \partial\Psi/\partial X = 0$ and $\Psi = 1$ at $|X| = \infty$. For a symmetric solitary ion wave structure, we can assume that $\Phi = \Phi_{max}$ and $\Psi = \Psi_{max}$, as well as $\partial\Psi/\partial X = \partial\Phi/\partial X = 0$ at $X = 0$. Hence, at $X = 0$, Eqn (84) yields

$$\Phi_{max}\Psi_{max}^2 + M\left(\sqrt{M^2 - 2\Phi_{max}} - M\right) = 0 \,. \tag{85}$$

In the wave-breaking limit, where $M = (2\Phi_{max})^{1/2}$, we find that $-\Phi_{max}\Psi_{max}^2 + 2\Phi_{max} = 0$, or $\Psi_{max} = 2$. Accordingly, the electron density locally increases to twice the background density at wave breaking.

In Fig. 7, numerical solutions of Eqns (82) and (83) are displayed, showing profiles of the electrostatic potential and electron number densities for different values of M. We see that both the electrostatic potential and the electron density have localized and strongly peaked maxima and an oscillatory tail. This is in sharp contrast to the classical (non-quantum) case, where the ion acoustic solitary waves have a monotonic profile, which in the small-amplitude limit, where the system is governed by the KdV equation, assumes a hyperbolic secant shape. We observe from Fig. 7 that $M = 1.1$ is close to the wave breaking limit above which solitary wave solutions do not exist. Our numerical investigation also suggests that there is a lower limit of M (slightly lower than 0.75), below which the solitary wave solution vanishes.

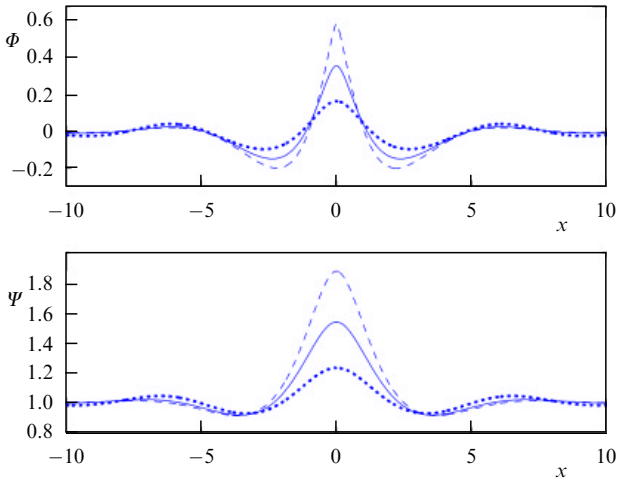

Figure 7. Profiles of the potential Φ (top panel) and the electron density Ψ^2 (bottom panel) as a function of X, for different values of the Mach number: $M = 1.1$ (dashed curves), $M = 0.9$ (solid curve), and $M = 0.75$ (dotted curve). From Ref. [62].

5. Quantum fluid turbulence

The statistical properties of turbulence and its associated electron transport at nanoscales in quantum plasmas have been investigated in both two and three dimensions by means of the coupled NLS and Poisson equations [66, 67]. It has been found that the nonlinear coupling between the EPOs of different scale sizes gives rise to small-scale electron density structures, while the electrostatic potential cascades toward large scales. The total energy associated with the quantum electron plasma turbulence nevertheless has a characteristic non-Kolmogorov-like spectrum. The electron diffusion caused by the electron fluid turbulence is consistent with the dynamical evolution of turbulent mode structures.

To investigate the quantum electron fluid turbulence in three dimensions, we use the nonlinear Schrödinger–Poisson equations [21, 22, 67]

$$i\sqrt{2H}\,\frac{\partial \Psi}{\partial t} + H\nabla^2\Psi + \varphi\Psi - |\Psi|^{4/3}\Psi = 0 \,, \tag{86}$$

$$\nabla^2\varphi = |\Psi|^2 - 1 \,, \tag{87}$$

which govern the dynamics of nonlinearly interacting EPOs of different wavelengths. In Eqns (86) and (87), the wave function is normalized by $\sqrt{n_0}$, the electrostatic potential by $k_B T_{Fe}/e$, the time t by the electron plasma period ω_{pe}^{-1}, and the space $\mathbf{r}$ by the Thomas–Fermi Debye radius V_{Fe}/ω_{pe}. We have introduced the notation $\sqrt{H} = \hbar\omega_{pe}/\sqrt{2}k_B T_{Fe}$.

Studies of the nonlinear mode coupling are aimed at investigating the multiscale evolution of a decaying 3D electron fluid turbulence, which is described by Eqns (86) and (87). All the fluctuations are initialized isotropically (no mean fields are assumed) with random phases and amplitudes in Fourier space, and evolve further through the integration of Eqns (86) and (87) using a fully de-aliased pseudospectral numerical scheme [154] based on the Fourier spectral methods. The spatial discretization in our 3D simulations uses a discrete Fourier representation of turbulent fluctuations. The numerical algorithm used here conserves energy in terms of the dynamical fluid variables and not due to a separate energy equation written in a conservative form.

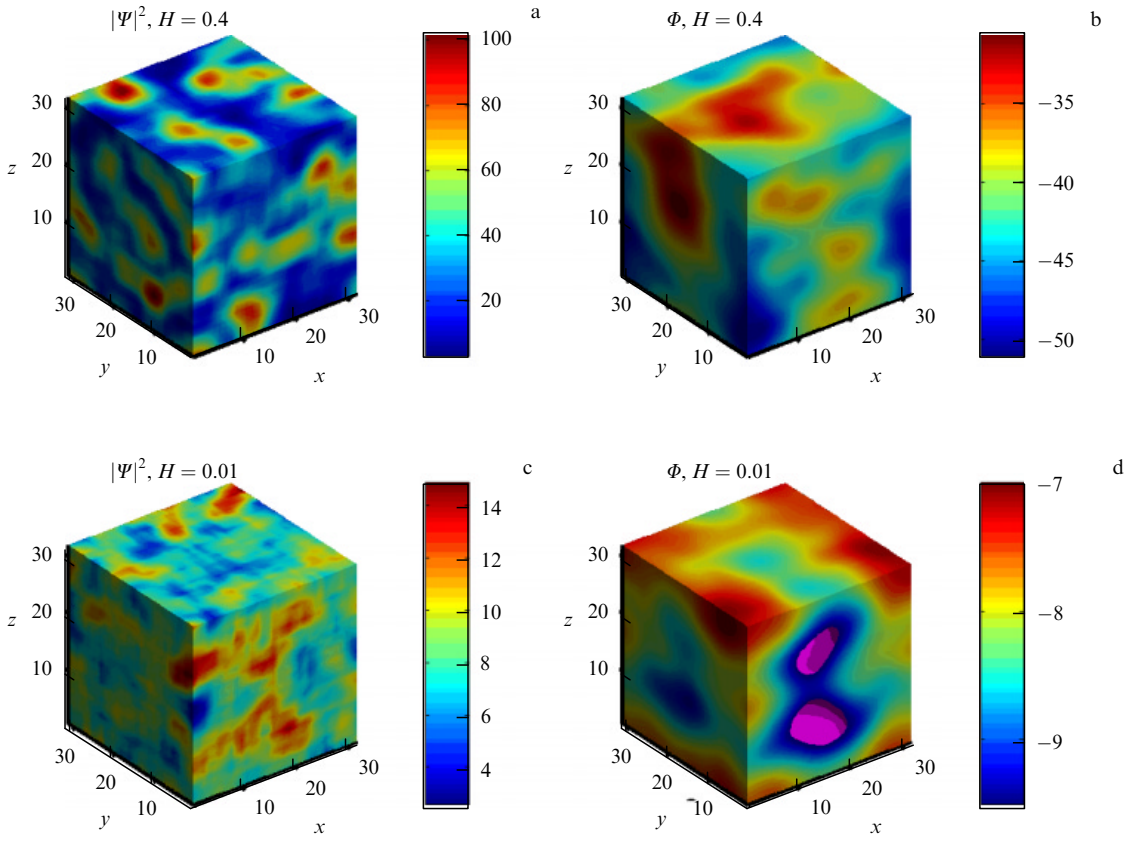

Figure 8. Small-scale fluctuations in the electron density resulting from a steady turbulence simulation of our 3D electron plasma, for $H = 0.4$ (top panels) and $H = 0.01$ (bottom panels). Forward cascades are responsible for the generation of small-scale fluctuations seen in panels (a) and (c). Large-scale structures are present in the electrostatic potential, seen in panels (b) and (d), essentially resulting from an inverse cascade. From Ref. [67].

The evolution variables use periodic boundary conditions. The initial isotropic turbulent spectrum was chosen close to k^{-2}, with random phases in all three directions. The choice of such a spectrum (or even a spectrum flatter than the k^{-2} one) treats the turbulent fluctuations on an equal footing and avoids any influence on the dynamic evolution that may be due to the initial spectral nonsymmetry. The equations are advanced in time using a second-order predictor–corrector scheme. The code is made stable by a proper de-aliasing of spurious Fourier modes and by choosing a relatively small time step in the simulations. Our code is massively parallelized using Message Passing Interface (MPI) libraries to facilitate higher resolution in a 3D computational box, with a resolution of 128^3 grid points.

We study the properties of 3D fluid turbulence, composed of nonlinearly interacting EPOs, for two specific physical systems: dense plasmas in the next-generation laser-based plasma compression (LBPC) schemes [81] and in superdense astrophysical objects [96–98] (e.g., white dwarfs). It is expected that in LBPC schemes, the electron number density may reach 10^{27} cm^{-3} and beyond. Hence, we have $\omega_{pe} = 1.76 \times 10^{18}$ s^{-1}, $T_F = 1.7 \times 10^{-9}$ erg, $\hbar\omega_{pe} = 1.7 \times 10^{-9}$ erg, and $H = 1$. The Fermi Debye length is $\lambda_D = 0.1$ Å. On the other hand, in the interior of white dwarfs, we typically have $n_0 \sim 10^{30}$ cm^{-3}, yielding $\omega_{pe} = 5.64 \times 10^{19}$ s^{-1}, $T_F = 1.7 \times 10^{-7}$ erg, $\hbar\omega_{pe} = 5.64 \times 10^{-8}$ erg, $H \approx 0.3$, and $\lambda_D = 0.025$ Å. The numerical solutions of Eqns (86) and (87) for $H = 1$ and $H = 0.025$ (respectively corresponding to $n_0 = 10^{27}$ cm^{-3} and $n_0 = 10^{30}$ cm^{-3}) are displayed in Figs 8 and 9, which are the electron number density and electrostatic (ES) potential distributions in the (x, y) plane.

Figures 8 and 9 reveal that the electron density distribution has a tendency to generate smaller-length scale structures, while the ES potential cascades toward larger scales. The coexistence of the small and larger scale structures in turbulence is a ubiquitous feature of various 3D turbulence systems. For example, in 3D hydrodynamic turbulence, the

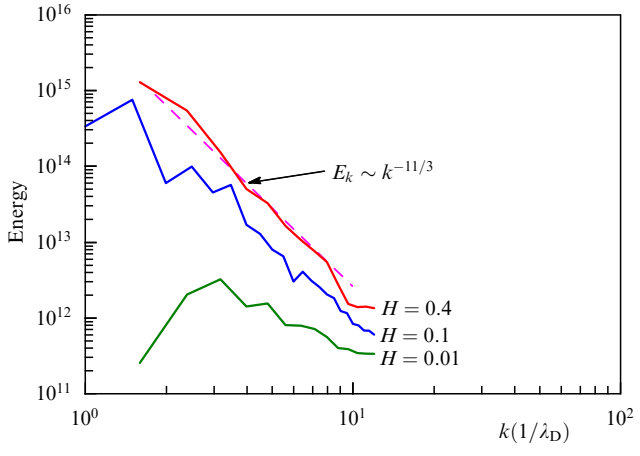

Figure 9. Power spectrum of 3D EPOs in the forward cascade regime. A Kolmogorov-like spectrum $\sim k^{-11/3}$ is observed for $H = 0.4$. The spectral index changes as a function of H. The numerical resolution is 128^3. From Ref. [67].

incompressible fluid admits two invariants, the energy and the mean squared vorticity. The two invariants, under the action of an external force, cascade simultaneously in turbulence, thereby leading to a dual cascade phenomenon. In these processes, the energy cascades toward longer length scales, while the fluid vorticity transfers spectral power toward shorter length scales. Usually, a dual cascade is observed in a driven turbulence simulation, in which certain modes are excited externally through random turbulent forces in spectral space. Randomly excited Fourier modes transfer the spectral energy by preserving the constants of motion in k-space. On the other hand, in freely decaying turbulence, the energy contained in large-scale eddies is transferred to the smaller scales, leading to a statistically stationary inertial regime associated with the forward cascades of one of the invariants. Decaying turbulence often leads to the formation of coherent structures as turbulence relaxes, thus making the nonlinear interactions rather inefficient when they are saturated. The power spectrum exhibits an interesting feature in our 3D electron plasma system, in contrast to the 3D hydrodynamic turbulence [155–158]. The spectral slope in the 3D quantum electron fluid turbulence is close to the Iroshnikov–Kraichnan power law $k^{-3/2}$ [159, 160], rather than the usual Kolmogorov power law $k^{-5/3}$ [155]. We further find that this scaling is not universal and is critically determined by the quantum tunneling effect. For instance, for a higher value $H = 1.0$, the spectrum flattens (see Fig. 9). Physically, the flatness (or deviation from the $k^{-5/3}$ law) results from the short-wavelength part of the EPO spectrum, which is controlled by the quantum tunneling effect associated with the Bohm potential. The peak in the energy spectrum can be attributed to the higher turbulent power residing in the EPO potential, which eventually leads to the generation of larger-scale structures, as the total energy encompasses both the electrostatic potential and electron density components. In our dual cascade process, there is a delicate competition between the EPO dispersions caused by the statistical pressure law (giving the $k^2 V_F^2$ term, which dominates at longer scales) and the quantum Bohm potential (giving the $\hbar^2 k^4/4m_e^2$ term, which dominates at shorter scales with respect to a source). Furthermore, it is interesting to note that exponents other than $k^{-5/3}$ have also been observed in numerical simulations [161, 162] of the Charney and 3D incompressible Navier–Stokes equations. The velocity statistics of quantum turbulence in superfluid ^{4}He was recently examined in [163], where it was found to be significantly different from classical turbulence due to the topological interactions of vortices that are different from those in classical fluids.

Finally, we estimate the electron diffusion coefficient in the presence of small and large scale turbulent EPOs in our quantum plasma. An effective electron diffusion coefficient caused by the momentum transfer can be calculated from $D_{\rm eff} = \int_0^\infty \langle \mathbf{P}(\mathbf{r}, t)\, \mathbf{P}(\mathbf{r}, t + t') \rangle \, dt'$, where $\mathbf{P}$ is electron momentum, the angular brackets denote spatial averages, and the ensemble averages are normalized to unit mass. The effective electron diffusion coefficient $D_{\rm eff}$ essentially relates the diffusion processes associated with random translational motions of electrons in nonlinear plasmonic fields. We compute $D_{\rm eff}$ in our simulations to measure the turbulent electron transport that is associated with the turbulent structures that we have reported herein. It follows that the effective electron diffusion is lower when the field perturbations are Gaussian. On the other hand, the electron diffusion rapidly increases, with the eventual formation of longer length scale structures, as shown in Fig. 10. The electron diffusion due to large-scale potential distributions in quantum plasmas substantially dominates, as depicted by the solid curve in Fig. 10. Furthermore, in the steady state, nonlinearly coupled EPOs form stationary structures, and $D_{\rm eff}$ eventually saturates. Thus, remarkably, an enhanced electron diffusion results primarily due to the emergence of large-scale potential structures in our 3D quantum plasma.

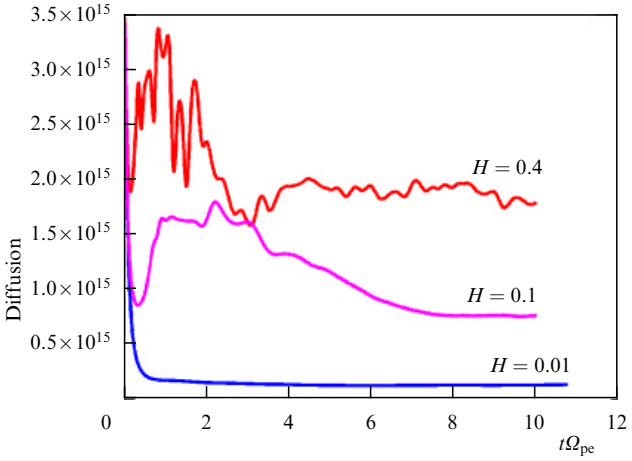

Figure 10. Time evolution of an effective electron diffusion coefficient associated with a large-scale electrostatic potential and a small-scale electron density, for $H = 0.4$, $H = 0.1$, and $H = 0.01$. Smaller values of H correspond to a small effective diffusion coefficient, which characterizes the presence of small-scale turbulent eddies that suppress the electron transport. From Ref. [67].

6. Kinetic phase-space structures

In the preceding sections, we discussed the properties of quantized coherent structures and 3D quantum electron fluid turbulence based on the coupled Schrödinger and Poisson equations. We assumed that nonlinearly interacting plasma waves are spontaneously created by some known physical processes (e.g., a beam–plasma instability) in quantum plasmas.

In classical plasmas, the formation of electrostatic kinetic phase-space structures based on the Vlasov–Poisson equations has been well documented [164]. In what follows, we discuss the quasilinear aspects [165] of the EPOs that are governed by the Wigner–Poisson system (i.e., a quantum analogue of the Vlasov–Poisson system). Specifically, we focus on kinetic phase-space nonlinear structures arising from the trapping of electrons in a finite-amplitude wave potential and a self-consistent modification of the electron distribution function in the presence of nano-kinetic structures.

To study the differences in the nonlinear evolution of the Wigner and Vlasov equations, we have simulated the well-known bump-on-tail instability [165], whereby a high-velocity beam is used to destabilize a Maxwellian equilibrium. We use the initial condition

$$f = (1 + \delta)\left(\frac{n_0}{\sqrt{2\pi} v_{\rm th}}\right)\left[0.8 \exp\left(-\frac{v^2}{2v_{\rm th}^2}\right) + 0.4 \exp\left(-\frac{2(v - 2.5v_{\rm th})^2}{v_{\rm th}^2}\right)\right],$$

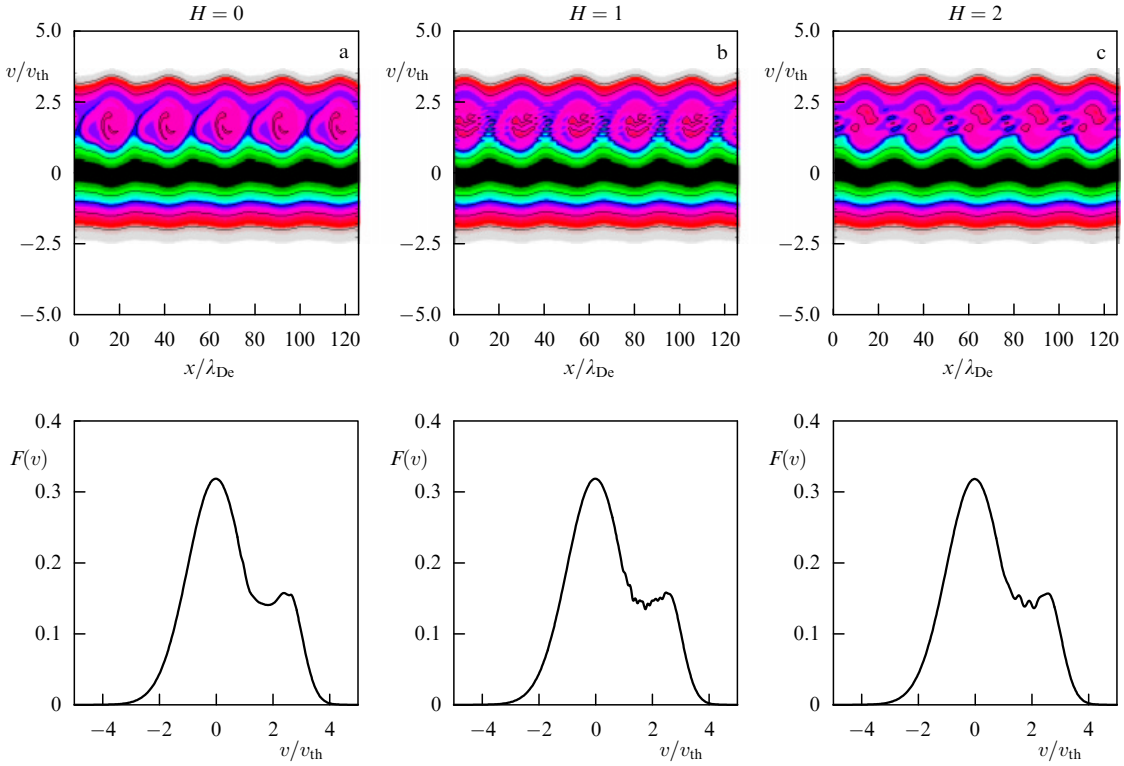

Figure 11. Simulations of the Wigner–Poisson and Vlasov–Poisson systems, at time $\omega_{pe}t = 200$, for a) $H = 0$ (Vlasov), b) $H = 1$ (Wigner), and c) $H = 2$ (Wigner). The spectrum is initially monochromatic. Top panels: the electron distribution function $f(x, v)$ in phase space. Bottom panels: the spatially averaged electron distribution function $F(v)$ in velocity space. From Ref. [165]. (A color version can be viewed online at www.ufn.ru)

where δ represents random fluctuations of the order of 10^{-5} that help seed the instability (see Fig. 11). Here, $v_{th} = \sqrt{k_B T_e/m_e}$ is the electron thermal speed. We use periodic boundary conditions with the spatial period $L = 40\pi\lambda_{De}$, where $\lambda_{De} = v_{th}/\omega_{pe}$ is the Debye length. Three simulations were performed, with different values of the normalized Planck constant defined as $H = \hbar\omega_{pe}/mv_{th}^2$: $H = 0$ (Vlasov), $H = 1$, and $H = 2$.

To highlight the transient oscillations in velocity space, we first perturb the above equilibrium with a monochromatic wave with $k\lambda_{De} = 0.25$ (i.e., the wavelength $8\pi\lambda_{De}$). Figure 11 shows the results of simulations of the Wigner–Poisson and Vlasov–Poisson systems. In both simulations, due to the bump-on-tail instability, electrostatic waves develop nonlinearly and create periodic trapped-particle islands (electron holes) with the wavenumber $k = 0.25\lambda_{De}^{-1}$. The theory predicts the formation of velocity-space oscillations in the Wigner evolution, which should be absent in the classical (Vlasov) simulations. This is the case with the results presented in Fig. 12, where the oscillations are clearly visible.

When the initial excitation is broad-band (i.e., wavenumbers $0.05 \leqslant k\lambda_{De} \leqslant 0.5$ are excited), the electron holes start merging at later times due to the sideband instability [166, 167] (see Fig. 12). At this stage, mode coupling becomes important and a quasilinear theory is not capable of describing these effects. As the system evolves toward a larger spatial wavelength, the evolution becomes progressively more classical, with the appearance of a plateau in the resonant region. Nevertheless, at $\omega_{pe}t = 500$, the Wigner solution still displays some oscillatory behavior in velocity space, which is absent in the Vlasov evolution.

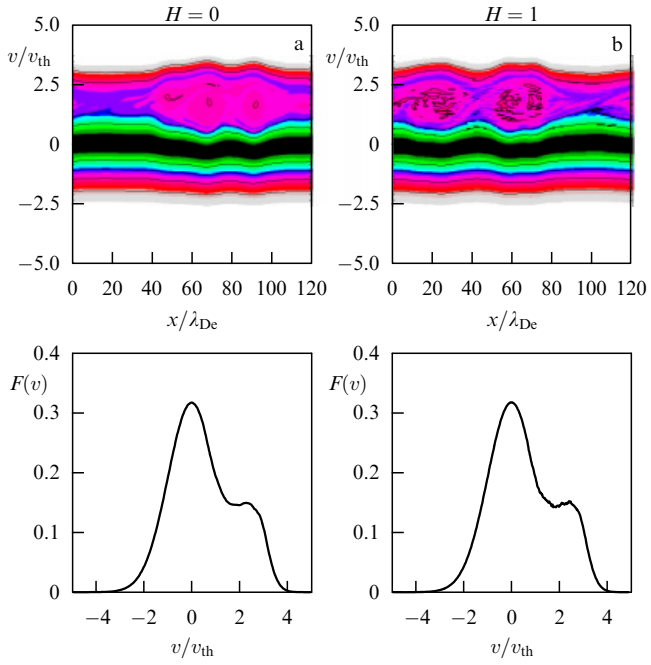

Figure 12. Simulations of the Wigner–Poisson and Vlasov–Poisson systems for $\omega_{pe}t = 500$, (a) for $H = 0$ (Vlasov) and (b) $H = 1$ (Wigner). The wavenumber spectrum was initially broad. Top panels: the electron distribution function $f(x, v)$ in phase space. Bottom panels: the spatially averaged electron distribution function $F(v)$ in velocity space. From Ref. [165]. (A color version can be viewed online at www.ufn.ru)

From the experimental standpoint, recent collective X-ray scattering observations in warm dense matter [118] revealed a measurable shift in the plasmon frequency due to quantum effects. In the nonlinear regime (strong excitations), this effect could lead to trapping of electrons in the wave potential of plasmons and the subsequent formation of the kind of phase-space structures discussed here. Furthermore, we note that there also exists a theoretical description [168] of quantum-corrected electron holes based on the perturbative treatment of the Wigner–Poisson equations.

7. Magnetic fields in quantum plasmas

Magnetic fields can be generated in classical plasmas via several mechanisms. These include (i) nonparallel density and temperature gradients (the so-called Biermann battery [169]), (ii) electron temperature anisotropy (known as the Weibel instability [170]), (iii) counterstreaming electron beams [171, 172], and (iv) the ponderomotive forces of laser beams [173–179].

In what follows, we discuss two possibilities for magnetic field generation in quantum plasmas.

7.1 Quantum Weibel instability

We first discuss linear and nonlinear aspects [180–183] of the Weibel instability that is driven by the equilibrium Fermi–Dirac electron temperature anisotropic distribution function in a nonrelativistic dense quantum plasma. It is well known [184] that a dense quantum plasma with an isotropic equilibrium distribution function does not allow any purely growing linear modes. This can be verified, for instance, from the expression for the imaginary part of the transverse dielectric function, derived in [185], for a fully degenerate nonrelativistic Fermi plasma. It can be proven (see Eqn (30) of [186]) that the only exception occurs for extremely small wavelengths, $k > 2k_{\mathrm{F}}$, where k_{F} is the characteristic Fermi wave number of the system. However, the wave would then be superluminal. On the other hand, in a classical Vlasov–Maxwell plasma containing an anisotropic electron distribution function, we have a purely growing Weibel instability [170], giving rise to DC magnetic fields. The electron temperature anisotropy may occur due to the heating of the plasma by laser beams [187], where a signature of the Weibel instability is present as well. In the next generation of intense laser–solid density plasma experiments, it is likely that electrons will be degenerate and that the electron temperature anisotropy may develop due to an anisotropic electron heating by intense laser beams via resonant absorption, similarly to the classical case of laser–plasma interaction [188].

We consider linear transverse waves in a dense quantum plasma composed of electrons and immobile ions, with $\mathbf{kE} = 0$, where $\mathbf{k}$ is the wave vector and $\mathbf{E}$ is the wave electric field. Following the standard procedure, we then obtain the general dispersion relation [1, 182, 183] for the transverse waves of the Wigner–Maxwell system:

$$\omega^2 - \omega_{\mathrm{pe}}^2 - k^2c^2 + \frac{m_{\mathrm{e}}\omega_{\mathrm{pe}}^2}{2n_0\hbar}\int \mathrm{d}\mathbf{v}\left(\frac{v_x^2+v_y^2}{\omega - kv_z}\right) \times\left[f_0\left(v_x, v_y, v_z + \frac{\hbar k}{2m}\right) - f_0\left(v_x, v_y, v_z - \frac{\hbar k}{2m_{\mathrm{e}}}\right)\right] = 0, \quad (88)$$

where $\mathbf{v} = (v_x, v_y, v_z)$ is the velocity vector and $f_0(v_x, v_y, v_z)$ is the equilibrium Wigner function associated with Fermi systems. For spin-1/2 particles, the equilibrium pseudo-distribution function has the form of a Fermi–Dirac function. Here, we allow the velocity anisotropy and write

$$f_0 = \frac{\alpha}{\exp\left\{m/2\left[(v_x^2+v_y^2)/\varkappa_{\mathrm{B}}T_\perp + v_z^2/\varkappa_{\mathrm{B}}T_\parallel\right] - \beta\mu\right\} + 1}, \quad (89)$$

where μ is the chemical potential and

$$\alpha = -\frac{n_0}{\mathrm{Li}_{3/2}[-\exp(\beta\mu)]}\left(\frac{m_{\mathrm{e}}\beta}{2\pi}\right)^{3/2} = 2\left(\frac{m_{\mathrm{e}}}{2\pi\hbar}\right)^3 \quad (90)$$

is the normalization constant. Here, $\mathrm{Li}_{3/2}$ is a polylogarithm function [189, 190]. Also, $\beta = 1/[\varkappa_{\mathrm{B}}(T_\perp^2 T_\parallel)^{1/3}]$, where $T_\perp$ and $T_\parallel$ are respectively related to the velocity dispersion in the direction perpendicular and parallel to the z axis. In the special case where $T_\perp = T_\parallel$, the usual Fermi–Dirac equilibrium is recovered. The chemical potential is obtained by solving normalization condition (90), which in particular yields $\mu = E_{\mathrm{F}}$ in the limit of zero temperature, where $E_{\mathrm{F}} = (3\pi^2 n_0)^{2/3}\hbar^2/(2m_{\mathrm{e}})$ is the Fermi energy. Also, the Fermi–Dirac distribution $\hat{f}(\mathbf{k})$, where $\mathbf{k}$ is the appropriate wave vector in momentum space, is related to equilibrium Wigner function (89) by $\hat{f}(\mathbf{k}) = (1/2)(2\pi\hbar/m)^3 f_0(\mathbf{v})$, with the factor 2 coming from spin [191, 192]. However, these previous works refer to the cases without temperature anisotropy. We note that it has been suggested in [193] that in laser plasmas, the Weibel instability is responsible for a further increase in $T_\parallel$ with time.

Substituting (89) in (90) and integrating over the perpendicular velocity components, we obtain

$$\omega^2 - k^2c^2 - \omega_{\mathrm{pe}}^2\left(1 + \frac{T_\perp}{T_\parallel}W_{\mathrm{Q}}\right) = 0, \quad (91)$$

where

$$W_{\mathrm{Q}} = \frac{1}{2\sqrt{\pi}H\,\mathrm{Li}_{3/2}[-\exp(\beta\mu)]}\int\frac{\mathrm{d}v}{v-\xi} \times\left(\mathrm{Li}_2\left\{-\exp\left[-\left(v+\frac{H}{2}\right)^2 + \beta\mu\right]\right\} - \mathrm{Li}_2\left\{-\exp\left[-\left(v-\frac{H}{2}\right)^2 + \beta\mu\right]\right\}\right). \quad (92)$$

In (92), Li_2 is the dilogarithm function [189, 190], $H = \hbar k/(m_{\mathrm{e}}v_\parallel)$ is a characteristic parameter representing the quantum diffraction effect, $\xi = \omega/(kv_\parallel)$, and $v = v_z/v_\parallel$, with $v_\parallel = (2\varkappa_{\mathrm{B}}T_\parallel/m_{\mathrm{e}})^{1/2}$. In the simultaneous limit of a small quantum diffraction effect ($H \ll 1$) and a dilute system ($\exp(\beta\mu) \ll 1$), it can be shown that $W_{\mathrm{Q}} \simeq -1 - \xi Z(\xi)$, where Z is the standard plasma dispersion function [194]. It is important that either (88) or (91) reproduces the transverse dielectric function calculated from the random-phase approximation for a fully degenerate quantum plasma [185] in the case of an isotropic system. A simple way to verify this equivalence is to set $T_\perp = T_\parallel$ in (88) and then take the limit of zero temperature, yielding $f_0 = 3n_0/(4\pi V_{\mathrm{Fe}}^3)$ for $|\mathbf{v}| < V_{\mathrm{Fe}}$ and $f_0 = 0$ otherwise.

We next solve our new dispersion relation (91) for a set of parameters that are representative of the next-generation laser–solid density plasma interaction experiments. Normalization condition (90) can also be written as

$-\mathrm{Li}_{3/2}[-\exp(\beta\mu)] = (4/3\sqrt{\pi})(\beta E_\mathrm{F})^{3/2}$, which is formally the same relation that holds for isotropic Fermi–Dirac equilibria [8]. For a given value of $\beta\mu$ times the density, this relation yields the value of β from which the temperatures $T_\perp$ and $T_\parallel$ can be calculated if $T_\perp/T_\parallel$ is known. We consider only purely growing modes. It follows from definition (92) that $W_\mathrm{Q} \to -1$ as $\omega = \mathrm{i}\gamma \to 0$ for a finite wavenumber k. From (91), we then obtain the maximum wavenumber for the instability as $k_\mathrm{max} = (\omega_\mathrm{pe}/c)\sqrt{T_\perp/T_\parallel - 1}$. As $T_\perp/T_\parallel \to 1$, the range of unstable wavenumbers shrinks to zero. In Figs 13 and 14, we use the electron number density $n_0 = 10^{33}$ m^{-3}, which can be obtained in laser-driven compression schemes. The growth rate for different values of $T_\perp/T_\parallel$ is displayed in Fig. 13. We see that the maximum unstable wavenumber is $k_\mathrm{max} = (\omega_\mathrm{pe}/c)\sqrt{T_\perp/T_\parallel - 1}$, as predicted, and that the maximum growth rate occurs at $k \approx k_\mathrm{max}/2$. Figure 13 also reveals that the maximum growth rate of the instability is almost linearly proportional to $T_\perp/T_\parallel - 1$. In Fig. 14, we have varied the product $\beta\mu$, which is a measure of the degeneracy of the quantum plasma. We see that for $\beta\mu$ larger than 5, the instability reaches a limit value, which is independent of the temperature, while thermal effects start playing an important role for $\beta\mu$ of the order of unity.

From several numerical solutions of the linear dispersion relation, an approximate scaling law was deduced [183] for the instability as $\gamma_\mathrm{max}/\omega_\mathrm{pe} = \mathrm{const} \times n_0^{1/3}(T_\perp/T_\parallel - 1)$, where the constant is approximately 8.5×10^{-14} m s^{-1}. Using

$$n_0 = \frac{(2m_\mathrm{e}E_\mathrm{F}/\hbar^2)^{3/2}}{3\pi^2} \approx 1.67 \times 10^{36}\left(\frac{E_\mathrm{F}}{m_\mathrm{e}c^2}\right)^{3/2},$$

we have

$$\frac{\gamma_\mathrm{max}}{\omega_\mathrm{pe}} = 0.10\left(\frac{E_\mathrm{F}}{m_\mathrm{e}c^2}\right)^{1/2}\left(\frac{T_\perp}{T_\parallel} - 1\right) \tag{93}$$

for the maximum growth rate of the Weibel instability in a degenerate Fermi plasma. This scaling law, where the growth rate depends on the Fermi energy and the temperature anisotropy, should be compared with that of a classical plasma [188, 195], where the growth rate depends on the thermal energy and the temperature anisotropy.

For a Maxwellian plasma, it has been found in [196] that the Weibel instability saturates nonlinearly as the magnetic bounce frequency $\omega_\mathrm{c} = eB/m_\mathrm{e}c$ increases to a value comparable to the linear growth rate. To assess the nonlinear behavior of the Weibel instability for a degenerate plasma, we have carried out a kinetic simulation of the Wigner–Maxwell system. We have assumed that the quantum diffraction effect is small, and hence the simulation of the Wigner equation can be approximated by simulations of the Vlasov equation by means of an electromagnetic Vlasov code [197]. As the initial condition for the simulation, we used distribution function (89). To give a seed for any instability, the plasma density was perturbed with low-frequency fluctuations (random numbers). The results are displayed in Figs 15 and 16 for the parameters $\beta\mu = 5$ and $T_\perp/T_\parallel = 2$ corresponding to the solid lines. Figure 15 shows the magnetic field components as a function of space and time. We see that the magnetic field initially increases and saturates to steady-state magnetic field fluctuations with the amplitude $eB/m_\mathrm{e}c\omega_\mathrm{pe} \approx 0.008$. The maximum amplitude of the magnetic field over the simulation box as a function of time is shown in Fig. 16, where we see that the magnetic field saturates at $eB/m_\mathrm{e}c\omega_\mathrm{pe} \approx 0.0082$, while the linear growth rate of the most unstable mode is $\gamma_\mathrm{max}/\omega_\mathrm{pe} \approx 0.009$. Similarly to the classical Maxwellian plasma case [196], we can thus estimate the generated magnetic field as

$$B = \frac{m_\mathrm{e}c\gamma_\mathrm{max}}{e} \tag{94}$$

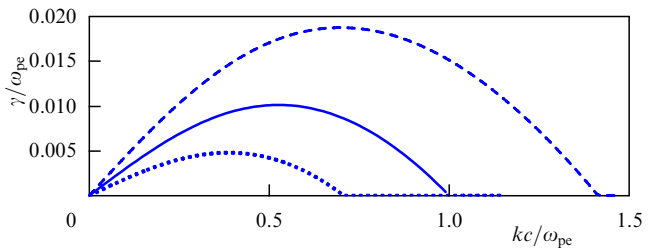

Figure 13. The growth rate for the Weibel instability of a dense fermionic plasma with $n_0 = 10^{33}$ m^{-3} ($\omega_\mathrm{pe} = 1.8 \times 10^{18}$ s^{-1}) and $\beta\mu = 5$, relevant for the next generation of inertially compressed materials in intense laser–solid density plasma interaction experiments. The temperature anisotropy is $T_\perp/T_\parallel = 3$ (dashed line), $T_\perp/T_\parallel = 2$ (solid line), and $T_\perp/T_\parallel = 1.5$ (dotted line), respectively yielding $T_\parallel = 3.9 \times 10^6$ K, $T_\parallel = 5.2 \times 10^6$ K, and $T_\parallel = 6.3 \times 10^6$ K. From Ref. [183].

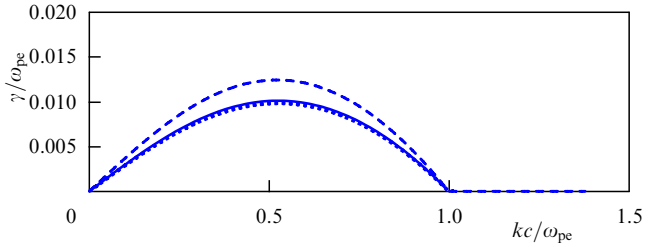

Figure 14. The growth rate for the Weibel instability of a dense fermionic plasma with $n_0 = 10^{33}$ m^{-3} ($\omega_\mathrm{pe} = 1.8 \times 10^{18}$ s^{-1}). The temperature anisotropy is $T_\perp/T_\parallel = 2$. We used $\beta\mu = 1$ (dashed line), $\beta\mu = 5$ (solid line), and $\beta\mu = 10$ (dotted line), respectively yielding $T_\parallel = 1.6 \times 10^7$ K, $T_\parallel = 5.2 \times 10^7$ K, and $T_\parallel = 2.6 \times 10^6$ K. From Ref. [183].

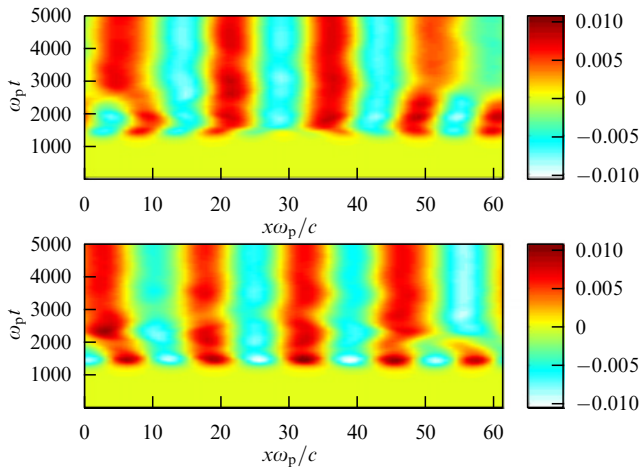

Figure 15. The magnetic field components B_y (top panel) and B_z (bottom panel) as a function of space and time, for $\beta\mu = 5$ and $T_\perp/T_\parallel = 2$. The magnetic field is normalized by $\omega_\mathrm{pe}m_\mathrm{e}/e$. We see a nonlinear saturation of the magnetic field components at the amplitude ~ 0.01. From Ref. [183].

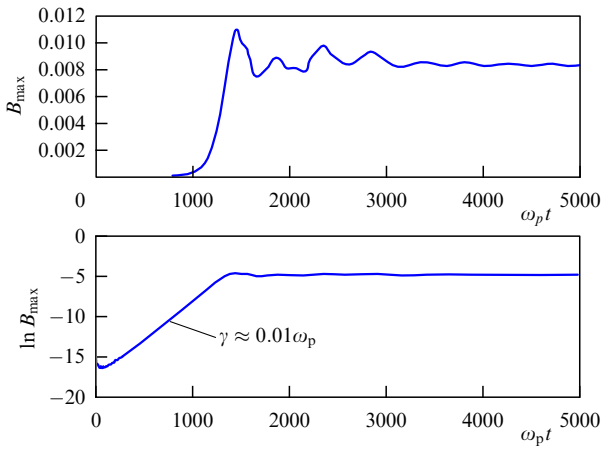

Figure 16. The maximum of the magnetic field amplitude $B = (B_y^2 + B_z^2)^{1/2}$ over the simulation box (top panel), and the logarithm of the magnetic field maximum (bottom panel) as a function of time, for $T_\perp/T_\parallel = 2$ and $\beta\mu = 5$. The magnetic field is normalized by $\omega_{pe}m_e/e$. From the logarithmic slope of the magnetic field in the linear regime, we find $\gamma \approx \Delta \ln(B_{max})/\Delta t \approx 0.01\,\omega_p$. From Ref. [183].

for a degenerate Fermi plasma. For our parameters, relevant for intense laser–solid interaction experiments, we thus have magnetic fields of the order of 10^5 T (one gigagauss).

7.2 Dense plasma magnetization by an electromagnetic wave

The second example of dense plasma magnetization can occur in the presence of streaming electrons and large amplitude electromagnetic waves. The nonstationary ponderomotive force of the electromagnetic wave would then create slowly varying electric fields and currents, which generate DC magnetic fields in dense plasmas.

We consider the propagation of an electromagnetic wave with the electric field $\mathbf{E}(\mathbf{r}, t) = (1/2)\mathbf{E}_0(x, t) \times \exp(-i\omega t + ikx) + \text{c.c.}$ in an unmagnetized nonrelativistic dense plasma with immobile ions and streaming electrons (with the drift velocity $u\hat{\mathbf{z}}$, where u is the magnitude of the electron drift speed and $\hat{\mathbf{z}}$ is the unit vector along the z axis in a Cartesian coordinate system; typically, u is much smaller than the electron Fermi speed). Here, $\mathbf{E}_0(x, t)$ is the envelope of the electromagnetic field at the position $\mathbf{r}$ and time t, and c.c. stands for complex conjugate. The frequency ω and the wave vector $\mathbf{k} = k\hat{\mathbf{x}}$, where $\hat{\mathbf{x}}$ is the unit vector along the x axis, are related by [198]

$$\frac{k^2c^2}{\omega^2} = N = 1 - \frac{\omega_{pe}^2}{\omega^2} - \frac{k^2u^2\omega_{pe}^2}{\omega^2(\omega^2 - k^2V_{Fe}^2 - \Omega_q^2)}\,, \tag{95}$$

where N is the refractive index and $\Omega_q = \hbar k^2/2m_e$.

The electromagnetic wave exerts a ponderomotive force $\mathbf{F}_p = \mathbf{F}_{ps} + \mathbf{F}_{pt}$ on the plasma electrons, where the stationary and nonstationary ponderomotive forces [173] are respectively given by

$$\mathbf{F}_{ps} = \frac{N-1}{16\pi}\,\nabla|\mathbf{E}_0|^2 \tag{96}$$

and

$$\mathbf{F}_{pt} = \frac{1}{16\pi}\,\frac{\mathbf{k}}{\omega^2}\,\frac{\partial\left[\omega^2(N-1)\right]}{\partial\omega}\,\frac{\partial|\mathbf{E}_0|^2}{\partial t}\,. \tag{97}$$

The ponderomotive force pushes the electrons locally, and creates the slowly varying electric field

$$\mathbf{E}_s = -\nabla\phi_s - \frac{1}{c}\,\frac{\partial\mathbf{A}_s}{\partial t} = \frac{1}{n_0e}\,\mathbf{F}_p\,, \tag{98}$$

where the scalar and vector potentials are

$$\phi_s = -\frac{N-1}{16\pi n_0e}\,|\mathbf{E}_0|^2\,, \tag{99}$$

and

$$\mathbf{A}_s = -\frac{c}{16\pi n_0e}\,\frac{\mathbf{k}}{\omega^2}\,\frac{\partial\left[\omega^2(N-1)\right]}{\partial\omega}\,|\mathbf{E}_0|^2\,. \tag{100}$$

The induced slowly varying magnetic field $\mathbf{B}_s$ is then $\mathbf{B}_s = \nabla \times \mathbf{A}_s$. Noting that

$$\frac{\partial\left[\omega^2(N-1)\right]}{\partial\omega} = \frac{2\omega k^2u^2\omega_{pe}^2}{(\omega^2 - k^2V_{Fe}^2 - \Omega_q^2)^2}\,, \tag{101}$$

we can express the magnitude of the magnetic field as

$$|\mathbf{B}_s| = \frac{eck^3u^2|\mathbf{E}_0|^2}{2m_eL\omega(\omega^2 - \Omega^2)^2}\,, \tag{102}$$

where L is the scale length of the $|\mathbf{E}_0|^2$ envelope and $\Omega = (k^2V_{Fe}^2 + \Omega_q^2)^{1/2} \equiv (\hbar k^2/2m_e)[1 + 4(3\pi^2n_0)^{2/3}/k^2]^{1/2}$. We note from (102) that the magnetic field strength is proportional to u^2 and attains a large value when $\omega \sim \Omega$. The electron gyrofrequency Ω_c is

$$\Omega_c = \frac{e|\mathbf{B}_s|}{m_ec} = \frac{k^3V_0^2u^2\omega}{2L(\omega^2 - \Omega^2)^2}\,, \tag{103}$$

where $V_0 = e|\mathbf{E}_0|/m_e\omega$ is the electron quiver velocity in the electromagnetic field.

8. Dynamics of electromagnetic waves in dense plasmas

We here consider various electromagnetic (EM) wave modes and their nonlinear interaction in dense plasmas. As examples, we discuss spin waves occuring in a magnetized plasma due to the spin-1/2 effect of electrons and positrons. We also consider nonlinear interactions between finite-amplitude electromagnetic and electrostatic waves in dense plasmas. We focus on the underlying physics of stimulated scattering instabilities and wave localization due to parametric interactions involving radiation pressure [178].

8.1 Electromagnetic spin waves in magnetized plasmas

In the presence of an external magnetic field, the quantum description of the linear kinetics of a dense collisionless plasma is complicated due to quantization of the gyromagnetic motion and the inclusion of the electron and positron spin 1/2. In the past, many authors [199–203] investigated high-frequency conductivity and the longitudinal and transverse dielectric responses in dense magnetized plasmas. The propagation characteristics of high-frequency electromagnetic waves in quantum magnetoplasmas are different from those in a classical magnetoactive plasma [204].

Recently, Oraevsky et al. [70] found a new electromagnetic spin wave whose electric field is parallel to $B_0\,\hat{\mathbf{z}}$ and which propagates across $\hat{\mathbf{z}}$, where $\hat{\mathbf{z}}$ is the unit vector along the z axis in a Cartesian coordinate system and B_0 is the strength of the ambient magnetic field. The spin wave accompanies the magnetization current due to spinning electron motion and the wave frequency is obtained from [70]

$$\frac{k_\perp^2 c^2}{\omega^2} = 1 - \frac{\omega_{\rm pe}^2}{\omega(\omega + {\rm i}\nu_{\rm e})} + 2\pi\mu_{\rm B}^2\,\frac{k_\perp^2 c^2 n_0}{\omega^2 E_{\rm F}}\,\frac{\omega_{\rm ce}}{\omega - \omega_{\rm ce}}\,, \quad (104)$$

where $k_\perp$ is the normal component of the wave vector $\mathbf{k} = k_\perp\hat{\mathbf{x}}$, $\hat{\mathbf{x}}$ is the unit vector transverse to $\hat{\mathbf{z}}$, $\nu_{\rm e}$ is the electron collision frequency, and $E_{\rm F} \sim m_{\rm e}c^2$. The third term in the right-hand side of (104) represents the electron spin-magnetic resonance at the electron gyrofrequency $\omega_{\rm ce} = eB_0/m_{\rm e}c$.

Assuming that $k_\perp^2 c^2 + \omega_{\rm pe}^2 \neq \omega_{\rm ce}^2$, we obtain from (104) that

$$\omega \simeq \omega_{\rm ce}\left[1 + \frac{2\pi\mu_{\rm B}^2 n_0}{E_{\rm F}}\,\frac{k_\perp^2 c^2}{k_\perp^2 c^2 + \omega_{\rm pe}^2(1 - {\rm i}\nu_{\rm e}/\omega) - \omega_{\rm ce}^2}\right]. \quad (105)$$

For $\nu_{\rm e} \ll \omega \sim \omega_{\rm ce}$, the damping rate of the spin mode is

$${\rm Im}\,\omega \simeq \frac{\nu_{\rm e}\omega_{\rm pe}^2 k_\perp^2 c^2 \mu_{\rm B}^2 B_0^2}{E_{\rm F} m_{\rm e} c^2 \omega_{\rm ce}^2 (k_\perp^2 c^2 + \omega_{\rm pe}^2 - \omega_{\rm ce}^2)^2}\,. \quad (106)$$

The ponderomotive force of the spin wave can create a compressional magnetic field perturbation due to an inverse Cotton–Mouton/Faraday effect [205].

8.2 Nonlinearly coupled EM waves

Finite-amplitude electromagnetic waves in quantum magnetoplasmas interact nonlinearly among themselves. In this subsection, we use the generalized Q-MHD equations to obtain compact nonlinear equations for the electron magnetohydrodynamic (EMHD) and Hall-MHD plasmas, and show how the density, the fluid velocity, and the magnetic field perturbations are coupled in a nontrivial manner.

The governing nonlinear equations for the electromagnetic waves in dense magnetoplasmas are the quantum magnetohydrodynamic equations: the continuity equation

$$\frac{\partial n_{\rm e,i}}{\partial t} + \nabla\cdot(n_{\rm e,i}\,\mathbf{u}_{\rm e,i}) = 0\,, \quad (107)$$

the electron and ion momentum equations

$$n_{\rm e}m_{\rm e}\left(\frac{\partial}{\partial t} + \mathbf{u}_{\rm e}\cdot\nabla\right)\mathbf{u}_{\rm e} = -n_{\rm e}e\left(\mathbf{E} + \frac{1}{c}\,\mathbf{u}_{\rm e}\times\mathbf{B}\right) - \nabla P_{\rm e} + \mathbf{F}_{\rm Qe}\,, \quad (108)$$

$$n_{\rm i}m_{\rm i}\left(\frac{\partial}{\partial t} + \mathbf{u}_{\rm i}\cdot\nabla\right)\mathbf{u}_{\rm i} = Z_{\rm i}en_{\rm i}\left(\mathbf{E} + \frac{1}{c}\,\mathbf{u}_{\rm i}\times\mathbf{B}\right), \quad (109)$$

the Faraday law

$$c\nabla\times\mathbf{E} = -\frac{\partial\mathbf{B}}{\partial t}\,, \quad (110)$$

and the Maxwell equation involving the magnetization spin current

$$\nabla\times\mathbf{B} = \frac{4\pi}{c}\left(\mathbf{J}_{\rm p} + \mathbf{J}_{\rm m}\right) + \frac{1}{c}\,\frac{\partial\mathbf{E}}{\partial t}\,, \quad (111)$$

where the pressure for nonrelativistic degenerate electrons is given by [206]

$$P_{\rm e} = \frac{4eB(2m_{\rm e})^{1/2}E_F^{3/2}}{3(2\pi)^2\hbar^2 c}\left[1 + 2\sum_{n_L=1}^{n_{\rm max}}\left(1 - \frac{n_L\hbar\omega_{\rm ce}}{E_{\rm F}}\right)^{3/2}\right], \quad (112)$$

with $n_L = 0, 1, 2, \ldots, n_{\rm max}$ and the value of $n_{\rm max}$ fixed by the largest integer n_L that satisfies $E_{\rm F} - n_L\hbar\omega_{\rm ce} \geqslant 0$.

The sum of the quantum Bohm and intrinsic angular momentum spin forces is

$$\mathbf{F}_{\rm Qe} = \nabla\left(\frac{\nabla^2\sqrt{n_{\rm e}}}{\sqrt{n_{\rm e}}}\right) - \frac{n_{\rm e}\,\mu_{\rm B}^2}{k_{\rm B}T_{\rm Fe}}\,\nabla B\,. \quad (113)$$

In Eqns (107)–(113), n_j is the number density of the particle species j (j equals e for electrons and i for ions), u_j is the particle fluid velocity, and $B = |\mathbf{B}|$. We introduced the plasma current density $\mathbf{J}_{\rm p} = -n_{\rm e}e\,\mathbf{u}_{\rm e} + Z_{\rm i}\,n_{\rm i}e\,\mathbf{u}_{\rm i}$ and the electron magnetization spin current density $\mathbf{J}_{\rm m} = \nabla\times\mathbf{M}$, where the magnetization for dynamics on a time scale much slower than the spin precession frequency for an electron Fermi gas is given by $\mathbf{M} = (n_{\rm e}\,\mu_{\rm B}^2/k_{\rm B}T_{\rm Fe})\,\hat{\mathbf{B}}$ [208].

8.2.1 Nonlinear EMHD. First, we present the generalized nonlinear EMHD equations for a dense magnetoplasma. Here, the ions form a neutralizing background. The wave phenomena in the EMHD plasma occur on a time scale much shorter than the ion plasma and ion gyroperiods. In equilibrium, we have

$$n_{\rm e0} = Z_{\rm i}n_{\rm i0} \equiv n_0\,. \quad (114)$$

The relevant nonlinear EMHD equations are

$$\frac{\partial n_{\rm e}}{\partial t} + \nabla\cdot(n_{\rm e}\mathbf{u}_{\rm e}) = 0\,, \quad (115)$$

with electron momentum equation (108), Faraday's law (110), and the electron fluid velocity being given by

$$\mathbf{u}_{\rm e} = \frac{\mathbf{J}_{\rm m}}{en_{\rm e}} - \frac{c(\nabla\times\mathbf{B})}{4\pi en_{\rm e}} + \frac{1}{en_{\rm e}}\,\frac{\partial\mathbf{E}}{\partial t}\,. \quad (116)$$

We observe that the quantum tunneling and spin forces play an important role if slight electron density and magnetic field inhomogeneities occur in a dense plasma. The nonlinear EMHD equations are useful for studying collective electron dynamics in metallic and semiconductor nanostructures [112].

8.2.2 Nonlinear Hall-MHD. Second, we derive the modified nonlinear Hall-MHD equations in a dense electron–ion plasma. The Hall-MHD equations deal with wave phenomena on a time scale larger than the electron gyroperiod. The relevant nonlinear Hall-MHD equations are the electron and ion continuity equations, the inertialess electron momentum equation

$$\mathbf{E} + \frac{1}{c}\,\mathbf{u}_{\rm e}\times\mathbf{B} - \frac{\nabla P_{\rm e}}{n_{\rm e}e} - \frac{\mathbf{F}_{\rm Qe}}{n_{\rm e}e} = 0\,, \quad (117)$$

Faraday's law (110), the ion momentum equation

$$n_{\rm i}m_{\rm i}\left(\frac{\partial}{\partial t} + \mathbf{u}_{\rm i}\cdot\nabla\right)\mathbf{u}_{\rm i} = Z_{\rm i}en_{\rm i}\left(\mathbf{E} + \frac{1}{c}\,\mathbf{u}_{\rm i}\times\mathbf{B}\right), \quad (118)$$

and the electron fluid velocity given by

$$\mathbf{u}_e = \mathbf{u}_i + \frac{\mathbf{J}_m}{en_e} - \frac{c(\nabla \times \mathbf{B})}{4\pi en_e}\,, \tag{119}$$

where we have neglected the displacement current because the Hall-MHD plasma deals with electromagnetic waves whose phase velocity is much smaller than the speed of light in the vacuum.

We now use (117) to eliminate the electric field from (118), which yields

$$n_i m_i \left(\frac{\partial}{\partial t} + \mathbf{u}_i \cdot \nabla\right)\mathbf{u}_i = Z_i e n_i \left[\frac{1}{c}(\mathbf{u}_i - \mathbf{u}_e) \times \mathbf{B} - \frac{\nabla P_e}{n_e e} + \frac{\mathbf{F}_{Qe}}{n_e e}\right]. \tag{120}$$

Furthermore, using (119) to eliminate $\mathbf{u}_e$ from (120), we have

$$n_i m_i \left(\frac{\partial}{\partial t} + \mathbf{u}_i \cdot \nabla\right)\mathbf{u}_i = Z_i e n_i \left\{\frac{1}{c}\left[-\frac{\mathbf{J}_m}{en_e} + \frac{c(\nabla \times \mathbf{B})}{4\pi}\right] \times \mathbf{B} - \frac{\nabla P_e}{n_e e} + \frac{\mathbf{F}_{Qe}}{n_e e}\right\}, \tag{121}$$

with the quasineutrality condition $n_e = Z_i n_i$. Finally, using (117), we can eliminate $\mathbf{E}$ from (108) to obtain

$$\frac{\partial \mathbf{B}}{\partial t} = \nabla \times \left[(\mathbf{u}_i \times \mathbf{B}) + \frac{\mathbf{J}_m \times \mathbf{B}}{eZ_i n_i} - \frac{c}{4\pi}(\nabla \times \mathbf{B}) \times \mathbf{B}\right]. \tag{122}$$

The ion continuity equation, Eqns (121) and (122), together with (118) and the relation $Z_i n_{i1} = n_{e1}$, where $n_{e1,i1} \ll n_{e0,i0}$, are the desired generalized nonlinear equations for the low-frequency (in comparison with the electron gyrofrequency), low phase velocity (in comparison with the speed of light in the vacuum) waves in a Hall-MHD dense plasma. They can be used to investigate the multidimensional linear and nonlinear waves (e.g., magnetosonic solitons [209]), as well as nanostructures and turbulence [210] in dense quantum magnetoplasmas.

8.3 Stimulated scattering instabilities

Nonlinear interactions between the high-frequency EM waves and low-frequency electrostatic waves give rise to stimulated scattering instabilities in classical plasmas [130, 211–213]. The possibility also exists of exciting plasma waves by high-frequency EM waves in quantum plasmas due to parametric instabilities [214]. The governing equations for the high-frequency electromagnetic waves [64] and the radiation-pressure-driven modified Langmuir and ion–acoustic oscillations in an unmagnetized quantum plasma are respectively given by

$$\left(\frac{\partial^2}{\partial t^2} - c^2\nabla^2 + \omega_{pe}^2\right)\mathbf{A} + \omega_{pe}^2 \frac{n_1}{n_0}\,\mathbf{A} \approx 0\,, \tag{123}$$

$$\left(\frac{\partial^2}{\partial t^2} + \omega_{pe}^2 - \frac{3}{5}\,V_{Fe}^2\nabla^2 + \frac{\hbar^2}{4m_e^2}\nabla^4\right)\frac{n_1}{n_0} = \frac{q_e^2}{2m_e^2c^2}\,\nabla^2|\mathbf{A}|^2 \tag{124}$$

and

$$\left(\frac{\partial^2}{\partial t^2} - \frac{m_e}{m_i}\,V_{Fe}^2\nabla^2 + \frac{\hbar^2}{4m_e m_i}\,\nabla^4\right)\frac{n_1}{n_0} = \frac{q_e^2}{2m_e m_i c^2}\,\nabla^2|\mathbf{A}|^2\,, \tag{125}$$

where $\mathbf{A}$ is the vector potential of a high-frequency electromagnetic wave and n_1 is the electron density perturbation of low-frequency oscillations (the modified EPOs and ion waves).

Combining Eqns (123)–(125), we thus simply obtain the nonlinear dispersion relations

$$\omega^2 - \Omega_R^2 = -\frac{q_e^2\omega_{pe}^2\,k^2|\mathbf{A}_0|^2}{2m_e^2c^2}\sum_{\pm}\frac{1}{D_\pm} \tag{126}$$

and

$$\omega^2 - \Omega_B^2 = -\frac{q_e^2\omega_{pe}^2\,k^2|\mathbf{A}_0|^2}{2m_e m_i c^2}\sum_{\pm}\frac{1}{D_\pm}\,, \tag{127}$$

where $\Omega_R = (\omega_{pe}^2 + 3k^2V_{Fe}^2/5 + \hbar^2k^4/4m_e^2)^{1/2}$ and $\Omega_B = (k^2C_{Fs}^2 + \hbar^2k^4/m_e m_i)^{1/2}$.

Equations (126) and (127) allow the stimulated Raman, stimulated Brillouin, and modulational instabilities of the electromagnetic pump (with the amplitude $\mathbf{A}_0$ and the frequency $\omega_0 = (k_0^2c^2 + \omega_{pe}^2)^{1/2}$) in dense quantum plasmas. We have set $D_\pm = \pm 2\omega_0(\omega - \mathbf{k}\,\mathbf{V}_g \mp \delta)$, where $\mathbf{V}_g = c^2\mathbf{k}_0/\omega_0$ is the group velocity of the EM pump wave frequency and $\delta = k^2c^2/2\omega_0$ is the small frequency shift arising from the nonlinear interaction of the pump with the electrostatic perturbations $(\omega, \mathbf{k})$ in our quantum plasma. For stimulated Raman and Brillouin scatterings, the EM pump wave is respectively scattered on the resonant electron plasma wave and resonant ion wave, while for the modulational instability, the electron and ion plasma oscillations are off-resonant, as are the EM sidebands.

For three-wave decay interactions, we suppose that $D_- = 0$ and $D_+ \neq 0$. Thus, we ignore D_+ in (126) and (127). Respectively setting $\omega = \Omega_R + i\gamma_R$ and $\omega = \Omega_B + i\gamma_B$ in (126) and (127) and assuming $\omega - \mathbf{k}\,\mathbf{V}_g + \delta \equiv i\gamma_{R,B}$, we obtain the growth rates for stimulated Raman and Brillouin scattering instabilities (denoted by the subscripts R and B):

$$\gamma_R = \frac{\omega_{pe}\,ek|\mathbf{A}_0|^2}{2\sqrt{2\omega_0\Omega_R}\,m_e c} \tag{128}$$

and

$$\gamma_B = \frac{\omega_{pe}\,ek|\mathbf{A}_0|^2}{2\sqrt{2\omega_0\Omega_B m_e m_i}\,c}\,, \tag{129}$$

where $|\mathbf{k}\,\mathbf{V}_g - \delta| \sim \Omega_R, \Omega_B$. We note that the growth rates for stimulated Raman and Brillouin scattering instabilities are inversely proportional to the square roots of Ω_R and Ω_B, which depend on the quantum parameters. Stimulated Raman and Brillouin scattering instabilities of the EM wave on the ES waves should provide invaluable information regarding the density fluctuations and the equation of states that might exist in dense quantum plasmas.

The quantum-corrected 3D Zakharov equations [127] have been derived by Haas [215] and Haas and Shukla [216], who demonstrated that the dispersive effects associated with quantum corrections can prevent the collapse of localized

Langmuir envelope electric fields in both two and three spatial dimensions.

8.4 Self-trapped EM waves in a quantum hole

Nonlinear interactions between large-amplitude electromagnetic waves and electrostatic plasma waves can produce nonlinear nanostructures composed of a density cavity that traps the electromagnetic wave envelope. Here, we demonstrate the trapping of intense electromagnetic waves in a finite-amplitude density hole [65] arising at a scale size of the order of the electron skin depth c/ω_{pe}.

A powerful circularly polarized electromagnetic (CPEM) plane wave interacting nonlinearly with the EPOs generates an envelope of the CPEM vector potential $\mathbf{A}_\perp = A_\perp(\hat{\mathbf{x}} + \mathrm{i}\hat{\mathbf{y}}) \times \exp(-\mathrm{i}\omega_0 t + \mathrm{i}k_0 z)$, which satisfies the nonlinear Schrödinger equation [178]

$$2\mathrm{i}\Omega_0\left(\frac{\partial}{\partial t} + V_g\frac{\partial}{\partial z}\right)A_\perp + \frac{\partial^2 A_\perp}{\partial z^2} - \left(\frac{|\psi|^2}{\gamma} - 1\right)A_\perp = 0\,, \tag{130}$$

where the electron wave function ψ and the scalar potential are governed by the equations

$$\mathrm{i}H_e\frac{\partial\psi}{\partial t} + \frac{H_e^2}{2}\frac{\partial^2\psi}{\partial z^2} + (\phi - \gamma + 1)\,\psi = 0 \tag{131}$$

and

$$\frac{\partial^2\phi}{\partial z^2} = |\psi|^2 - 1\,, \tag{132}$$

and where the electron number density is defined by the $|\psi|^2$ term. Here, Ω_0 represents the CPEM wave frequency, V_g is the x component of the group velocity of the CPEM wave, H_e is a quantum coupling parameter, and $\gamma = (1 + |A_\perp|^2)^{1/2}$ is the relativistic gamma factor due to the electron quiver velocity in the CPEM wave fields. The details of normalization of the variables are given in Ref. [65]. The nonlinear coupling between intense CPEM waves and EPOs occurs due to the nonlinear current density, which is represented by the term $|\psi|^2 A_\perp/\gamma$ in Eqn (130). In Eqn (131), $1 - \gamma$ is the relativistic ponderomotive potential [178], which arises due to the cross coupling between the CPEM wave-induced electron quiver velocity and the CPEM wave magnetic field.

The effect of quantum dispersion on localized electromagnetic pulses can be studied by considering a steady-state structure moving with a constant speed V_g. Inserting the ansatz $A_\perp = W(\xi)\exp(-\mathrm{i}\Omega t)$, $\psi = P(\xi)\exp(\mathrm{i}kx - \mathrm{i}\omega t)$, and $\phi = \phi(\xi)$ into Eqns (130)–(132), where $\xi = z - V_g t$, $k = V_g/H_e$, and $\omega = V_g^2/2H_e$, and where $W(\xi)$ and $P(\xi)$ are real, we obtain the coupled system of equations

$$\frac{\partial^2 W}{\partial\xi^2} + \left(\lambda - \frac{P^2}{\gamma} + 1\right)W = 0\,, \tag{133}$$

$$\frac{H_e^2}{2}\frac{\partial^2 P}{\partial\xi^2} + (\phi - \gamma + 1)\,P = 0, \tag{134}$$

where $\gamma = (1 + W^2)^{1/2}$, and

$$\frac{\partial^2\phi}{\partial\xi^2} = P^2 - 1 \tag{135}$$

with the boundary conditions $W = \Phi = 0$ and $P^2 = 1$ at $|\xi| = \infty$. In Eqn (133), $\lambda = 2\Omega_0\Omega$ represents a nonlinear frequency shift of the CPEM wave. In the limit $H_e \to 0$, it follows from (134) that $\phi = \gamma - 1$, where $P \neq 0$, and we recover the classical (nonquantum) case of relativistic solitary waves in a cold plasma [217]. System of equations (133)–(135) admits the Hamiltonian

$$Q_H = \frac{1}{2}\left(\frac{\partial W}{\partial\xi}\right)^2 + \frac{H_e^2}{2}\left(\frac{\partial P}{\partial\xi}\right)^2 - \frac{1}{2}\left(\frac{\partial\phi}{\partial\xi}\right)^2 + \frac{1}{2}(\lambda + 1)\,W^2 + P^2 - \gamma P^2 + \phi P^2 - \phi = 0\,, \tag{136}$$

where the boundary conditions $\partial/\partial\xi = 0$, $W = \phi = 0$, and $|P| = 1$ at $|\xi| = \infty$ have been used.

Numerical solutions of quasistationary system (133)–(135) are presented Figs 17 and 18, while time-dependent solutions of Eqns (130)–(132) are shown in Figs 19 and 20. Here, parameters were used that are representative of the next generation of laser-based plasma compression (LBPC) schemes [13, 14, 81]. The formula [178] $eA_\perp/mc^2 = 6\times10^{-10}\lambda_s\sqrt{I}$ determines the normalized vector potential if the CPEM wavelength λ_s (in microns) and the intensity I (in W cm^2) are known. It is expected that in LBPC schemes, the electron number density n_0 may reach 10^{27} cm^{-3} and beyond, and the peak values of $eA_\perp/mc^2$ may be in the range 1–2 (e.g., for focused EM pulses with $\lambda_s \sim 0.15$ nm and $I \sim 5\times10^{27}$ W cm^2). For $\omega_{pe} = 1.76\times10^{18}$ s^{-1}, we have $\hbar\omega_{pe} = 1.76\times10^{-9}$ erg and $H_e = 0.002$, because $mc^2 = 8.1\times10^{-7}$ erg. The electron skin depth is $\lambda_e \sim 1.7$ Å. On the other hand, a higher value $H_e = 0.007$ is achieved for $\omega_{pe} = 5.64\times10^{18}$ s^{-1}. Therefore, our numerical solutions below, based on these two values of H_e, are focused on scenarios that are relevant for the next generation of intense laser-solid density plasma interaction experiments [81].

Figures 17 and 18 show numerical solutions of Eqns (133)–(135) for several values of H_e. The nonlinear boundary value problem was solved with the boundary

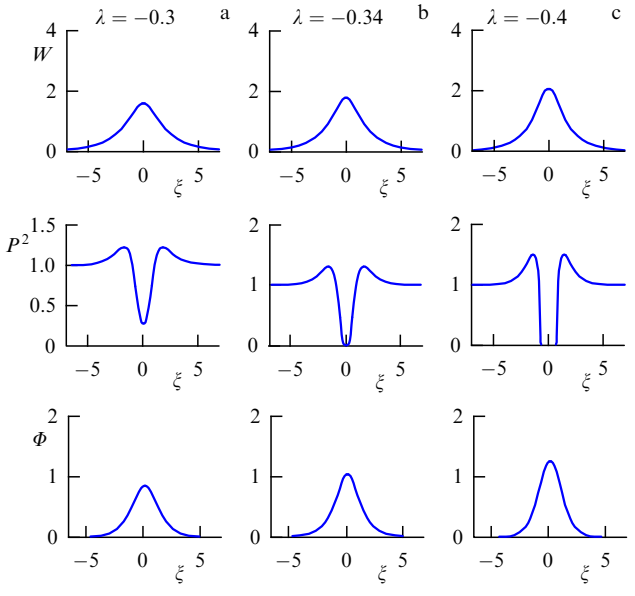

Figure 17. Profiles of the CPEM vector potential W (top row), the electron number density P^2 (middle row), and the scalar potential Φ (bottom row) for $\lambda = -0.3$ (left column), $\lambda = -0.34$ (middle column), and $\lambda = -0.4$ (right column), with $H_e = 0.002$. From Ref. [65].

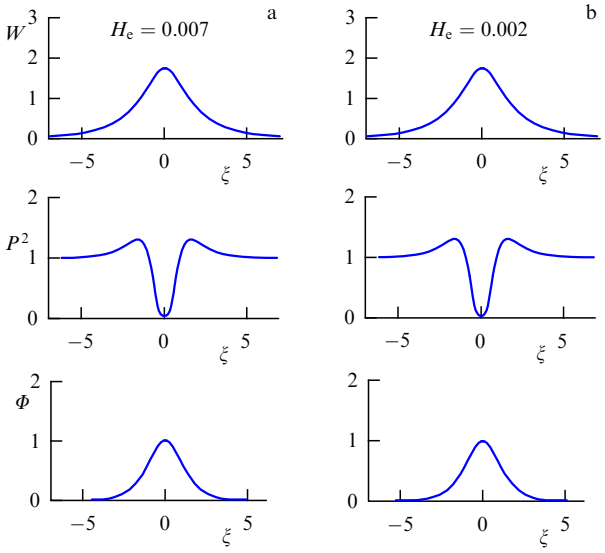

Figure 18. Profiles of the CPEM vector potential W (top row), the electron number density P^2 (middle row), and the scalar potential Φ (bottom row) for $H_e = 0.007$ (left column) and $H_e = 0.002$ (right column), with $\lambda = -0.34$. From Ref. [65].

conditions $W = \phi = 0$ and $P = 1$ at the boundaries at $\xi = \pm 10$. It follows that the solitary envelope pulse is composed of a single maximum of the localized vector potential W, a local depletion of the electron density P^2, and a localized positive potential ϕ at the center of the solitary pulse. The pulse has a continuous spectrum in λ, where larger values of negative λ are associated with larger-amplitude solitary EM pulses. At the center of the solitary EM pulse, the electron density is partially depleted, as in panels a) in Fig. 17; for larger amplitudes of the EM waves, a stronger depletion of the electron density occurs, as shown in panels b) and c) in Fig. 17. In the cases where the electron density almost tends to zero in the classical case [217], one important quantum effect is that the electrons can tunnel into the depleted region. This is seen in Fig. 18, where the electron density remains nonzero for the larger value of H_e in panels a) but shrinks to zero for the smaller value of H_e in panels b).

Figures 19 and 20 show numerical simulation results of Eqns (130)–(132), with the aim to investigate the quantum diffraction effects on the dynamics of localized CPEM wavepackets. The long-wavelength limit $\omega_0 \approx 1$ and $V_g \approx 0$ is considered here. As the initial conditions, an EM pump with the constant amplitude $A_\perp = A_0 = 1$ and the uniform plasma density $\psi = 1$ is used, together with a small-amplitude noise (random numbers) of the order of 10^{-2} added to $A_\perp$ to give a seeding any instability. The numerical results are displayed in Figs 19 and 20 for the respective values $H_e = 0.002$ and $H_e = 0.007$. In both cases, we can see an initial linear growth phase and a wave collapse at $t \approx 70$, in which almost all the CPEM wave energy is contracted into a few well-separated localized CPEM wave pipes. These are characterized by a large bell-shaped amplitude of the CPEM wave, an almost complete depletion of the electron number density at the center of the CPEM wavepacket, and a large-amplitude positive electrostatic potential. Comparing Fig. 19 with Fig. 20, we see that there are more complex dynamics in the interaction between the CPEM wavepackets for the larger value $H_e = 0.007$ in Fig. 19 than for $H_e = 0.002$ in Fig. 19,

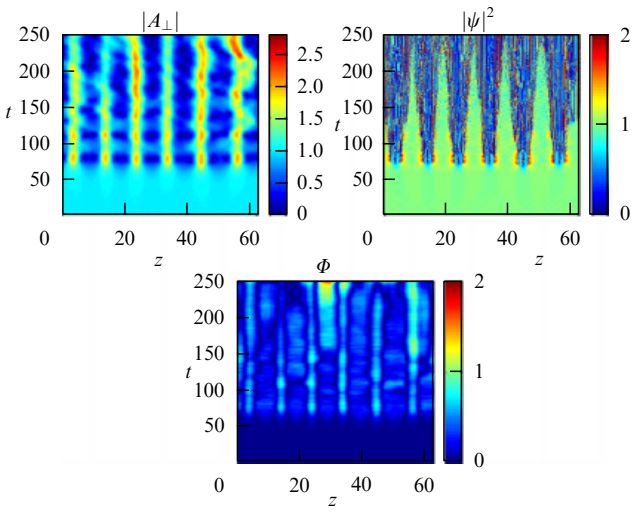

Figure 19. Dynamics of the CPEM vector potential $A_\perp$ and the electron number density $|\psi|^2$ (upper panels) and of the electrostatic potential Φ (lower panel) for $H_e = 0.002$. From Ref. [65].

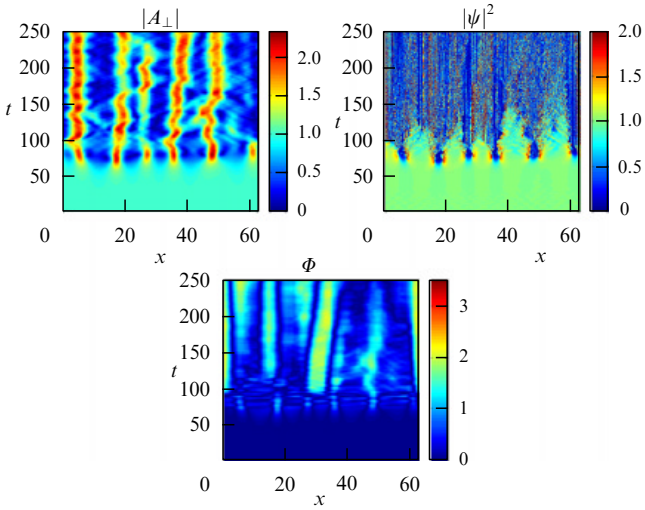

Figure 20. Dynamics of the CPEM vector potential $A_\perp$ and the electron number density $|\psi|^2$ (upper panels) and the electrostatic potential Φ (lower panel) for $H_e = 0.007$. From Ref. [65].

where the wavepackets are almost stationary when they are fully developed.

9. Summary and prospects

In this paper, we have presented our up-to-date theoretical knowledge of nonlinear physics of nonrelativistic quantum plasmas. We started with nonlinear quantum models that describe the physics of localized excitations in different areas of physics. We then discussed the well-known electron and ion plasma wave spectra in dense quantum plasmas, and presented nonlinear models for treating nonlinear interactions among finite-amplitude plasma waves at nanoscales. As examples, we demonstrated the existence of localized nonlinear EPOs and localized ion waves in dense quantum plasmas. For electrostatic EPOs, the electron dynamics is governed by a pair composed of nonlinear Schrödinger and Poisson (NLSP) equations. We stress that the nonlinear Schrödinger equation governing the spatio–temporal evolution of the electron wave function in the presence of a self-

consistent electrostatic potential in dense plasmas was obtained from the quantum electron momentum equation by introducing the eikonal representation as a mathematical tool for understanding the complex electron plasma wave interactions at nanoscales. Such a description also appears in the context of nonlinear electron dynamics in thin metal films [112]. Our NLSP equations admit a set of conserved quantities: the total number of electrons, the electron momentum, the electron angular momentum, and the electron energy. We have found that the NLSP equations admit quasistationary, localized structures in the form of one-dimensional quantized dark solitons and two-dimensional quantized vortices. These nanostructures are associated with a local depletion of the electron density associated with a positive electrostatic potential, and are parameterized by the quantum coupling parameter only. In the two-dimensional geometry, there exists a class of vortices of different excited states (charge states) associated with a complete depletion of the electron density and an associated positive potential. Numerical simulations of the time-dependent NLSP equations demonstrate the stability of stable dark solitons in one spatial dimension with an amplitude consistent with the one found from time-independent solutions. In two spatial dimensions, the dark solitons of the first excited state were found to be stable and the preferred nonlinear state was in the form of vortex pairs of different polarities. One-dimensional dark solitons and single charged two-dimensional vortices are thus long-lived nonlinear structures in quantum plasmas.

Similarly to the Bernstein–Green–Kruskal modes [164], we accounted for the trapping of electrons in the electrostatic wave potential and numerically studied the deformation of the equilibrium Fermi–Dirac distribution function and the subsequent emergence of localized phase-space kinetic structures. This was investigated using the time-dependent Wigner and Poisson equations. Furthermore, we presented two mechanisms for generation of magnetic fields in quantum plasmas. They are associated with the quantum Weibel instability in the presence of the equilibrium anisotropic Fermi–Dirac electron distribution function and with the nonstationary ponderomotive force of a large-amplitude electromagnetic wave in quantum plasmas with streaming electrons. Spontaneously generated magnetic fields can affect the linear and nonlinear propagation of both electrostatic and electromagnetic waves in quantum magnetoplasmas [39]. The quantum corrections produce dispersion at short scales for the electrostatic upper-hybrid, lower-hybrid, and ion-cyclotron waves, while the quantum Bohm force and the electron spin-1/2 effects introduce new features to the elliptically polarized extraordinary electromagnetic mode [40]. Furthermore, the electron spin 1/2 is responsible for a new electromagnetic spin wave propagating normally to the magnetic field direction, which can be excited by intense neutrino bursts in supernovae. The newly derived nonlinear EMHD and Hall-MHD equations can be used for investigating the multidimensional linear and nonlinear electromagnetic waves in quantum plasmas. Finally, we have also presented theoretical and numerical studies of stimulated Raman and Brillouin scattering instabilities of a large-amplitude electromagnetic wave, and the trapping of arbitrarily large amplitude circularly polarized EM waves in a fully nonlinear electron density hole in an unmagnetized quantum plasma. It is expected that localized nanostructures can transport electromagnetic wave energy over nanoscales in laboratory and astrophysical dense plasmas with degenerate electrons.

The field of nonlinear quantum plasma physics is extremely rich and vibrant today, and it holds great promise for providing new practical technologies. For example, plasma assisted carbon nanostructures and nanomaterials are the future of nanotechnologies, as are the new radiation sources in the X-ray and gamma-ray regimes. In such circumstances, it is desirable to fully understand the fundamentals of collective nonlinear interactions (e.g., intense high-order harmonic generation of ultrashort laser pulses from laser-irradiated dense plasma surfaces) in quantum plasmas. Furthermore, in magnetars and in the next generation of intense laser–solid density plasma interaction experiments, we would certainly have degenerate positrons, in addition to degenerate electrons. The physics of dense quantum magnetoplasmas with degenerate electron–positron pairs is expected to be quite different from what has been described in this paper. The reason is the complex nonlinear dynamics of the electron–positron pairs, which would have relativistic velocities in a dense magnetoplasma. Accordingly, we should develop new theories involving relativistic kinetic and quantum relativistic magnetohydrodynamic equations that include quantum relativistic effects [218 – 220], electromagnetic forces, angular momentum spin, and nonlinear effects on equal footings. A detailed analysis of such theories would provide us with a guideline for understanding the origin of localized high-energy radiation and other complex phenomena (e.g., the formation of structures) from astrophysical settings and future laboratory experiments aiming to model astrophysical scenarios.

Acknowledgements. One of the authors (P K Shukla) acknowledges the benefit of useful discussions with Academician and Professor Vladimir Fortov. We greatly appreciate our invaluable collaborations with Lennart Stenflo, Gert Brodin, Mattias Marklund, Fernando Haas, and Nitin Shukla.

This research was supported in part by the Deutsche Forschungsgemeinschaft (Bonn, Germany) under project SH21/3-1 of the Research Unit 1048, and by the Swedish Research Council (VR).

10. Appendix

10.1 Derivation of the Vlasov equation from the Wigner equation

We here show that the Wigner equation converges to the Vlasov equation in the classical limit $\hbar \to 0$. The Wigner equation is given by

$$\frac{\partial f}{\partial t} + \mathbf{v}\cdot\nabla f = -\frac{iem_e^3}{(2\pi)^3\hbar^4}\iint \mathrm{d}^3\lambda\,\mathrm{d}^3v'\exp\left[\mathrm{i}\frac{m_e}{\hbar}(\mathbf{v}-\mathbf{v}')\boldsymbol{\lambda}\right] \times\left[\phi\left(\mathbf{x}+\frac{\boldsymbol{\lambda}}{2},t\right)-\phi\left(\mathbf{x}-\frac{\boldsymbol{\lambda}}{2},t\right)\right]f(\mathbf{x},\mathbf{v}',t). \quad (137)$$

Changing the variable as $\boldsymbol{\lambda} = \hbar\boldsymbol{\xi}/m_e$ we have $\mathrm{d}^3\lambda = \hbar^3\,\mathrm{d}^3\xi/m_e^3$, and Eqn (137) takes the form

$$\frac{\partial f}{\partial t} + \mathbf{v}\cdot\nabla f = -\frac{\mathrm{i}e}{(2\pi)^3\hbar}\iint \mathrm{d}^3\xi\,\mathrm{d}^3v'\exp\left[\mathrm{i}(\mathbf{v}-\mathbf{v}')\boldsymbol{\xi}\right] \times\left[\phi\left(\mathbf{x}+\frac{\hbar\boldsymbol{\xi}}{2m_e},t\right)-\phi\left(\mathbf{x}-\frac{\hbar\boldsymbol{\xi}}{2m_e},t\right)\right]f(\mathbf{x},\mathbf{v}',t)\,. \quad (138)$$

Assuming that $\hbar/m_e$ is small, we expand ϕ in a Taylor series around $\mathbf{x}$ through the third order,

$$\phi\left(\mathbf{x} \pm \frac{\hbar\xi}{2m_e}, t\right) \approx \phi(\mathbf{x},t) \pm \frac{\hbar}{2m_e}(\xi\cdot\nabla)\,\phi(\mathbf{x},t) + \frac{\hbar^2}{8m_e^2}(\xi\cdot\nabla)^2\phi(\mathbf{x},t) \pm \frac{\hbar^3}{48m_e^3}(\xi\cdot\nabla)^3\phi(\mathbf{x},t), \quad (139)$$

whence

$$\frac{\partial f}{\partial t} + \mathbf{v}\cdot\nabla f \approx -\frac{\mathrm{i}e}{(2\pi)^3 m_e}\iint \mathrm{d}^3\xi\,\mathrm{d}^3v'\exp\left[\mathrm{i}(\mathbf{v}-\mathbf{v}')\,\xi\right] \times\left[\xi\cdot\nabla\phi(\mathbf{x},t) + \frac{\hbar^2}{24m_e^2}(\xi\cdot\nabla)^3\phi(\mathbf{x},t)\right] f(\mathbf{x},\mathbf{v}',t). \quad (140)$$

From the identity

$$\exp\left[\mathrm{i}(\mathbf{v}-\mathbf{v}')\,\xi\right]\xi = \mathrm{i}\nabla_{\mathbf{v}'}\exp\left[\mathrm{i}(\mathbf{v}-\mathbf{v}')\,\xi\right], \quad (141)$$

where $\nabla_{\mathbf{v}'} = \hat{\mathbf{x}}\partial/\partial v_x' + \hat{\mathbf{y}}\partial/\partial v_y' + \hat{\mathbf{z}}\partial/\partial v_z'$, we have

$$\frac{\partial f}{\partial t} + \mathbf{v}\cdot\nabla f = \frac{e}{(2\pi)^3 m_e}\iint \mathrm{d}^3\xi\,\mathrm{d}^3v'\left\{\exp\left[\mathrm{i}(\mathbf{v}-\mathbf{v}')\,\xi\right] \times\left[(\overleftarrow{\nabla}_{\mathbf{v}'}\cdot\overrightarrow{\nabla}) - \frac{\hbar^2}{24m_e^2}(\overleftarrow{\nabla}_{\mathbf{v}'}\cdot\overrightarrow{\nabla})^3\right]\phi(\mathbf{x},t)\right\} f(\mathbf{x},\mathbf{v}',t), \quad (142)$$

where the arrows indicate the direction of action of the nabla operators.

Integration by parts in $\mathbf{v}'$ space, with $f \to 0$ as $|\mathbf{v}'| \to \infty$, now yields

$$\frac{\partial f}{\partial t} + \mathbf{v}\cdot\nabla f = -\frac{e}{(2\pi)^3 m_e}\iint \mathrm{d}^3\xi\,\mathrm{d}^3v'\exp\left[\mathrm{i}(\mathbf{v}-\mathbf{v}')\,\xi\right] \times\left\{\phi(\mathbf{x},t)\left[(\overleftarrow{\nabla}\cdot\overrightarrow{\nabla}_{\mathbf{v}'}) - \frac{\hbar^2}{24m_e^2}(\overleftarrow{\nabla}\cdot\overrightarrow{\nabla}_{\mathbf{v}'})^3\right] f(\mathbf{x},\mathbf{v}',t)\right\}. \quad (143)$$

The integration in ξ space can now be formally performed, with the result

$$\frac{\partial f}{\partial t} + \mathbf{v}\cdot\nabla f = -\frac{e}{m_e}\int \mathrm{d}^3v'\,\delta(\mathbf{v}-\mathbf{v}') \times\left\{\phi(\mathbf{x},t)\left[(\overleftarrow{\nabla}\cdot\overrightarrow{\nabla}_{\mathbf{v}'}) - \frac{\hbar^2}{24m_e^2}(\overleftarrow{\nabla}\cdot\overrightarrow{\nabla}_{\mathbf{v}'})^3\right] f(\mathbf{x},\mathbf{v}',t)\right\}, \quad (144)$$

where the identity

$$\int \mathrm{d}^3\xi\exp\left[\mathrm{i}(\mathbf{v}-\mathbf{v}')\,\xi\right] = (2\pi)^3\delta(\mathbf{v}-\mathbf{v}') \quad (145)$$

was used (and where δ is the Dirac delta function). Finally, integration over $\mathbf{v}'$ space yields

$$\frac{\partial f}{\partial t} + \mathbf{v}\cdot\nabla f = -\frac{e}{m_e}\left\{\phi(\mathbf{x},t) \times\left[(\overleftarrow{\nabla}\cdot\overrightarrow{\nabla}_{\mathbf{v}}) - \frac{\hbar^2}{24m_e^2}(\overleftarrow{\nabla}\cdot\overrightarrow{\nabla}_{\mathbf{v}})^3\right] f(\mathbf{x},\mathbf{v},t)\right\}. \quad (146)$$

In the limit $\hbar \to 0$, we recover the Vlasov equation

$$\frac{\partial f}{\partial t} + \mathbf{v}\cdot\nabla f = -\frac{e}{m_e}\nabla\phi(\mathbf{x},t)\cdot\nabla_{\mathbf{v}} f(\mathbf{x},\mathbf{v},t). \quad (147)$$

10.2 Derivation of the dispersion relation for the Wigner–Poisson system

We here derive the dispersion relation for electrostatic waves in a degenerate quantum plasma governed by the Wigner–Poisson system of equations. The linearized Wigner–Poisson system of equations is given by

$$\frac{\partial f_1}{\partial t} + \mathbf{v}\cdot\nabla f_1 = -\frac{\mathrm{i}em_e^3}{(2\pi)^3\hbar^4}\iint \mathrm{d}^3\lambda\,\mathrm{d}^3v'\exp\left[\mathrm{i}\,\frac{m_e}{\hbar}(\mathbf{v}-\mathbf{v}')\,\boldsymbol{\lambda}\right] \times\left[\phi_1\left(\mathbf{x}+\frac{\boldsymbol{\lambda}}{2},t\right) - \phi_1\left(\mathbf{x}-\frac{\boldsymbol{\lambda}}{2},t\right)\right] f_0(\mathbf{v}'), \quad (148)$$

and

$$\nabla^2\phi_1 = 4\pi e\int f_1\,\mathrm{d}^3v, \quad (149)$$

where f_0 denotes the background distribution function, and f_1 and ϕ_1 respectively denote the perturbed distribution function and the electrostatic potential. Using the Fourier transformation for (148) and (149) in space and the Laplace transformation in time, we obtain

$$(\omega - \mathbf{k}\,\mathbf{v})f_1 = \frac{em_e^3}{(2\pi)^3\hbar^4}\iint \mathrm{d}^3\lambda\,\mathrm{d}^3v'\exp\left[\mathrm{i}\frac{m_e}{\hbar}(\mathbf{v}-\mathbf{v}')\,\boldsymbol{\lambda}\right] \times\left[\exp\left(\mathrm{i}\,\frac{\mathbf{k}\,\boldsymbol{\lambda}}{2}\right) - \exp\left(-\mathrm{i}\,\frac{\mathbf{k}\,\boldsymbol{\lambda}}{2}\right)\right] f_0(\mathbf{v}')\,\phi_1(\omega,\mathbf{k}), \quad (150)$$

$$k^2\phi_1 = -4\pi e\int f_1\,\mathrm{d}^3v. \quad (151)$$

Rewriting (150) as

$$(\omega - \mathbf{k}\,\mathbf{v})f_1 = \frac{\mathrm{i}em_e^3}{(2\pi)^3\hbar^4}\iint \mathrm{d}^3\lambda\,\mathrm{d}^3v' \times\left\{\exp\left[\frac{m_e}{\hbar}(\mathbf{v}-\mathbf{v}')\,\boldsymbol{\lambda} + \mathrm{i}\,\mathbf{k}\,\frac{\boldsymbol{\lambda}}{2}\right] - \exp\left[\mathrm{i}\,\frac{m_e}{\hbar}(\mathbf{v}-\mathbf{v}')\,\boldsymbol{\lambda} - \mathrm{i}\,\mathbf{k}\,\frac{\boldsymbol{\lambda}}{2}\right]\right\} f_0(\mathbf{v}')\,\phi_1(\omega,\mathbf{k}) \quad (152)$$

and integrating over $\boldsymbol{\lambda}$ space, we have

$$(\omega - \mathbf{v}\,\mathbf{k})f_1 = \frac{em_e^3}{\hbar^4}\int \mathrm{d}^3v'\left\{\delta\left[\frac{m_e}{\hbar}(\mathbf{v}-\mathbf{v}') + \frac{\mathbf{k}}{2}\right] - \delta\left[\frac{m_e}{\hbar}(\mathbf{v}-\mathbf{v}') - \frac{\mathbf{k}}{2}\right]\right\} f_0(\mathbf{v}')\,\phi_1(\omega,\mathbf{k}). \quad (153)$$

Now, the integration can be performed over $\mathbf{v}'$ space, yielding the result

$$(\omega - \mathbf{k}\,\mathbf{v})f_1 = \frac{e}{\hbar}\left[f_0\left(\mathbf{v}+\frac{\hbar\mathbf{k}}{2m_e}\right) - f_0\left(\mathbf{v}-\frac{\hbar\mathbf{k}}{2m_e}\right)\right]\phi_1(\omega,\mathbf{k}). \quad (154)$$

Solving Eqn (154) for f_1 and substituting the result in (151), we obtain the dispersion relation

$$1-\frac{4\pi e^2k^2}{\hbar}\times\int\left[\frac{f_0(\mathbf{v}+\hbar\mathbf{k}/2m_e)}{(-\omega+\mathbf{k}\,\mathbf{v})}-\frac{f_0(\mathbf{v}-\hbar\mathbf{k}/2m_e)}{(-\omega+\mathbf{k}\,\mathbf{v})}\right]\mathrm{d}^3v=0. \tag{155}$$

Suitable changes of variables in the two terms now give

$$1-\frac{4\pi e^2k^2}{\hbar}\int\left[\frac{1}{\left[-\omega+\mathbf{k}(\mathbf{u}-\hbar\mathbf{k}/2m_e)\right]}-\frac{1}{\left[-\omega+\mathbf{k}(\mathbf{u}+\hbar\mathbf{k}/2m_e)\right]}\right]f_0(\mathbf{u})\,\mathrm{d}^3u=0\,, \tag{156}$$

which can be rewritten as

$$1-\frac{4\pi e^2}{m_e}\int\frac{f_0(\mathbf{u})}{(\omega-\mathbf{k}\,\mathbf{u})^2-\hbar^2k^4/4m_e^2}\,\mathrm{d}^3u=0\,. \tag{157}$$

Dispersion relation (157) was also derived in [3] via a series of canonical transformations of the Hamiltonian of the system (see, e.g., Eqn (57) in [3]). We now choose a coordinate system such that the x axis is aligned with the wave vector $\mathbf{k}$. Then (157) takes the form

$$1-\frac{4\pi e^2}{m_e}\int\frac{f_0(\mathbf{u})}{(\omega-ku_x)^2-\hbar^2k^4/4m_e^2}\,\mathrm{d}^3u=0\,. \tag{158}$$

We next consider a dense plasma with degenerate electrons in the zero-temperature limit. Then the background distribution function takes the simple form

$$f_0=\begin{cases}2\left(\dfrac{m_e}{2\pi\hbar}\right)^3, & |\mathbf{u}|\leqslant V_{Fe}\,,\\ 0\,, & \text{elsewhere,}\end{cases} \tag{159}$$

where $V_{Fe}=(2E_{Fe}/m_e)^{1/2}$ is the speed of an electron on the Fermi surface, and $E_{Fe}=(3\pi^2n_0)^{2/3}\hbar^2/(2m_e)$ is the Fermi energy. The integration in (158) can be performed over the space of velocities perpendicular to u_x, using the cylindrical coordinate in u_y and u_z, with the result

$$1=\frac{4\pi e^2}{m_e}\int\frac{F_0(u_x)}{(\omega-ku_x)^2-(\hbar^2k^4)/4m_e^2}\,\mathrm{d}u_x\,, \tag{160}$$

where

$$F_0(u_x)=\iint f_0(\mathbf{u})\,\mathrm{d}u_y\,\mathrm{d}u_z=2\pi\int_0^{\sqrt{V_{Fe}^2-u_x^2}}2\left(\frac{m_e}{2\pi\hbar}\right)^3u_\perp\,\mathrm{d}u_\perp=\begin{cases}2\pi\left(\dfrac{m_e}{2\pi\hbar}\right)^3(V_{Fe}^2-u_x^2)\,, & |u_x|\leqslant V_{Fe},\\ 0\,, & \text{elsewhere.}\end{cases} \tag{161}$$

Equation (160) can be written as

$$1=\frac{8\pi^2e^2}{m_e}\left(\frac{m_e}{2\pi\hbar}\right)^3\int_{-V_{Fe}}^{V_{Fe}}\frac{V_{Fe}^2-u_x^2}{(\omega-ku_x)^2-(\hbar^2k^4)/4m_e^2}\,\mathrm{d}u_x=\frac{3\omega_{pe}^2}{4V_{Fe}^3}\int_{-V_{Fe}}^{V_{Ve}}\frac{V_{Fe}^2-u_x^2}{(\omega-ku_x)^2-(\hbar^2k^4)/4m_e^2}\,\mathrm{d}u_x\,. \tag{162}$$

First, in the limit as $\hbar k/m_e\to0$, it follows from (162) that

$$1+\frac{3\omega_{pe}^2}{k^2V_{Fe}^2}\left(1-\frac{\omega}{2kV_{Fe}}\log\left|\frac{\omega+kV_{Fe}}{\omega-kV_{Fe}}\right|\right)=0\,, \tag{163}$$

where we assume that ω is real and $\omega/k>V_{Fe}$.

Expanding (163) for small wavenumbers through terms containing k^2, we have

$$\omega^2=\omega_{pe}^2+\frac{3}{5}\,k^2V_{Fe}^2\,. \tag{164}$$

Second, for nonzero $\hbar k^2/m_e$, Eqn (162) implies the dispersion relation

$$1+\frac{3\omega_{pe}^2}{4k^2V_{Fe}^2}\left\{2-\frac{m_e}{\hbar kV_{Fe}}\left[V_{Fe}^2-\left(\frac{\omega}{k}+\frac{\hbar k}{2m_e}\right)^2\right]\times\log\left|\frac{\omega/k-V_{Fe}+(\hbar k)/2m_e}{\omega/k+V_{Fe}+(\hbar k)/2m_e}\right|+\frac{m_e}{\hbar kV_{Fe}}\times\left[V_{Fe}^2-\left(\frac{\omega}{k}-\frac{\hbar k}{2m_e}\right)^2\right]\log\left|\frac{\omega/k-V_{Fe}-(\hbar k)/2m_e}{\omega/k+V_{Fe}-(\hbar k)/2m_e}\right|\right\}=0. \tag{165}$$

Expanding (165) for small wavenumbers through terms containing k^4, we obtain

$$\omega^2\approx\omega_{pe}^2+\frac{3}{5}\,k^2V_{Fe}^2+(1+\alpha)\frac{\hbar^2k^4}{4m_e^2}\,, \tag{166}$$

where $\alpha=(48/175)\,m_e^2V_{Fe}^4/\hbar^2\omega_{pe}^2\approx2.000(n_0a_0^3)^{1/3}$ and $a_0=\hbar^2/m_ee^2\approx53\times10^{-10}$ cm is the Bohr radius. For a typical metal such as gold, whose free-electron number density is $n_0=5.9\times10^{22}$ cm^{-3}, we then have $\alpha\approx0.4$. For the free-electron density in semiconductors that is many orders of magnitude less than in metals, α is much smaller and can safely be dropped compared to unity.

References

1. Klimontovich Yu L, Silin V P *Dokl. Akad. Nauk SSSR* **82** 361 (1952); *Zh. Eksp. Teor. Fiz.* **23** 151 (1952)
2. Bohm D *Phys. Rev.* **85** 166 (1952)
3. Bohm D, Pines D *Phys. Rev.* **92** 609 (1953)
4. Pines D *J. Nucl. Energy Pt. C Plasma Phys.* **2** 5 (1961)
5. Bohm D, Pines D, in *Plasma Physics* (Ed. J E Drummond) (New York: McGraw-Hill, 1961) Ch. 2, p. 35
6. Bonitz M et al. *J. Phys. A Math. Gen.* **36** 5921 (2003)
7. Manfredi G *Fields Inst. Commun.* **46** 263 (2005)
8. Bransden B H, Joachain C J *Quantum Mechanics* 2nd ed. (Harlow: Prentice Hall, 2000)
9. Fortov V E, Iakubov I T *The Physics of Non-Ideal Plasma* (Singapore: World Scientific, 2000)
10. Lee T D *Astrophys. J.* **111** 625 (1950)
11. Hubbard W B *Astrophys. J.* **146** 858 (1966)
12. Lampe M *Phys. Rev.* **170** 306 (1968)
13. Azechi H et al. *Laser Part. Beams* **9** 193 (1991)
14. Azechi H et al. (the FIREX Project) *Plasma Phys. Control. Fusion* **48** B267 (2006)
15. Son S, Fisch N J *Phys. Rev. Lett.* **95** 225002 (2005)
16. Wigner E *Phys. Rev.* **40** 749 (1932)
17. Moyal J E *Proc. Camb. Philos. Soc.* **45** 99 (1949)
18. Anderson D et al. *Phys. Rev. E* **65** 046417 (2002)
19. Tsintsadze N L, Tsintsadze L N, arXiv:0903.5368
20. Gardner C L, Ringhofer C *Phys. Rev. E* **53** 157 (1996)
21. Manfredi G, Haas F *Phys. Rev. B* **64** 075316 (2001)
22. Shukla P K, Eliasson B *Phys. Rev. Lett.* **96** 245001 (2006)
23. Shukla P K *Phys. Lett. A* **352** 242 (2006)

24. Shukla P K, Eliasson B *New J. Phys.* **9** 98 (2007)
25. Maafa N *Phys. Scripta* **48** 351 (1993)
26. Melrose D B *Quantum Plasmadynamics: Unmagnetized Plasmas* (New York: Springer, 2008)
27. Lifshitz E M, Pitaevskii L P *Fizicheskaya Kinetika* (Physical Kinetics) (Moscow: Nauka, 1979) [Translated into English (Oxford: Butterworth-Heinemann, 1981)]
28. Nozieres P, Pines D *The Theory of Quantum Liquids* (Cambridge: Perseus Books, 1999) p. 279
29. Kremp D et al. *Phys. Rev. E* **60** 4725 (1999)
30. Bonitz M *Quantum Kinetic Theory* (Stuttgart: B.G. Teubner, 1998)
31. Kremp D, Schlanges M, Kraeft W-D *Quantum Statistics of Nonideal Plasmas* (Berlin: Springer, 2005)
32. Uhlenbeck G E, Goudsmit S *Naturwissenschaften* **47** 953 (1925); *Nature* **117** 264 (1926)
33. Bohm D *Quantum Theory* (New York: Prentice-Hall, 1951)
34. Sasabe S, Tsuchiya K *Phys. Lett. A* **372** 381 (2008)
35. Landau L D, Lifshitz E M *Kvantovaya Mekhanika: Nerelyativistskaya Teoriya* (Quantum Mechanics: Non-Relativistic Theory) (Moscow: Nauka, 1974) 3rd ed. [Translated into English (Oxford: Pergamon Press, 1977)]
36. Steinberg M *Thermodynamics and Kinetics of a Magnetized Quantum Plasma* (Berlin: Logos, 2000)
37. John P *Contrib. Plasma Phys.* **33** 488 (2006)
38. Shukla P K, Stenflo L *J. Plasma Phys.* **72** 605 (2006)
39. Shukla P K et al. *Phys. Plasmas* **13** 112111 (2006)
40. Shukla P K *Phys. Lett. A* **369** 312 (2007)
41. Lundin J et al. *Phys. Plasmas* **14** 062112 (2007)
42. Misra A P *Phys. Plasmas* **14** 064501 (2007)
43. Khan S A, Saleem H *Phys. Plasmas* **16** 052109 (2009)
44. Madelung E *Z. Phys.* **40** 322 (1927)
45. Takabayasi T *Prog. Theor. Phys.* **8** 143 (1952)
46. Takabayasi T *Prog. Theor. Phys.* **14** 283 (1955)
47. Takabayasi T *Prog. Theor. Phys.* **70** 1 (1983)
48. Bohm D, Schiller R, Tiomno J *Suppl. Nuovo Cimento* **1** 48 (1955)
49. Bohm D, Schiller R *Suppl. Nuovo Cimento* **1** 67 (1955)
50. Janossy L, Ziegler-Naray M *Acta Phys. Hung.* **20** 23 (1965)
51. Ghosh S K, Deb B M *Phys. Rep.* **92** 1 (1982)
52. Takabayasi T *Prog. Theor. Phys.* **9** 187 (1953)
53. Takabayasi T *Prog. Theor. Phys.* **13** 222 (1955)
54. Takabayasi T *Nuovo Cimento* **3** 233 (1956)
55. Takabayasi T *Prog. Theor. Phys. Suppl.* (4) 2 (1957)
56. Bialynicki-Birula I *Acta Phys. Polonica B* **26** 1201 (1995)
57. Gardner C L *SIAM J. Appl. Math.* **54** 409 (1994)
58. Loffredo M I, Morato L M *Nuovo Cimento B* **108** 205 (1993)
59. Feynman R P *Statistical Mechanics; A Set of Lectures* (Reading, Mass.: W.A. Benjamin, 1972) [Translated into Russian (Moscow: Mir, 1978)]
60. Domps A, Reinhard P-G, Suraud E *Phys. Rev. Lett.* **80** 5520 (1998)
61. Haas F, Garcia L G, Goedert J, Manfredi G *Phys. Plasmas* **10** 3858 (2003)
62. Eliasson B, Shukla P K *J. Plasma Phys.* **74** 581 (2008)
63. Haas F *Phys. Plasmas* **12** 062117 (2005)
64. Shukla P K, Stenflo L *Phys. Plasmas* **13** 044505 (2006)
65. Shukla P K, Eliasson B *Phys. Rev. Lett.* **99** 096401 (2007)
66. Shaikh D, Shukla P K *Phys. Rev. Lett.* **99** 125002 (2007)
67. Shaikh D, Shukla P K *New J. Phys.* **10** 083007 (2008)
68. Bershadskii A *Phys. Lett. A* **372** 2741 (2008)
69. Eliasson B, Shukla P K *Phys. Scr.* **78** 025503 (2008)
70. Oraevsky V N, Semikoz V B *Yad. Fiz.* **66** 494 (2003) [*Phys. At. Nucl.* **66** 466 (2003)]; Oraevsky V N, Semikoz V B, Volokitin A S, hep-ph/0203020
71. Marklund M, Brodin G *Phys. Rev. Lett.* **98** 025001 (2007)
72. Brodin G, Marklund M *Phys. Rev. E* **76** 055403(R) (2007)
73. Shukla P K, Stenflo L *J. Plasma Phys.* **74** 719 (2008)
74. Shukla P K *Nature Phys.* **5** 92 (2009)
75. Oraevsky V N, Semikoz V B *Astropart. Phys.* **18** 261 (2002)
76. Hu S X, Keitel C H *Phys. Rev. Lett.* **83** 4709 (1999)
77. Andreev A V *Pis'ma Zh. Eksp. Teor. Fiz.* **72** 350 (2000) [*JETP Lett.* **72** 238 (2000)]
78. Mourou G A, Tajima T, Bulanov S V *Rev. Mod. Phys.* **78** 309 (2006)
79. Marklund M, Shukla P K *Rev. Mod. Phys.* **78** 591 (2006)
80. Salamin Y A et al. *Phys. Rep.* **427** 41 (2006)
81. Malkin V M, Fisch N J, Wurtele J S *Phys. Rev. E* **75** 026404 (2007)
82. Kritcher A L et al. *Science* **322** 69 (2008)
83. Hartemann F V, Siders C W, Barty C P J *Phys. Rev. Lett.* **100** 125001 (2008)
84. Lee H J et al. *Phys. Rev. Lett.* **102** 115001 (2009)
85. Norreys P A et al. *Phys. Plasmas* **16** 041002 (2009)
86. Drake R P *Phys. Plasmas* **16** 055501 (2009)
87. van Horn H M *Science* **252** 384 (1991)
88. Guillot T *Science* **286** 72 (1999)
89. Fortney J J et al. *Phys. Plasmas* **16** 041003 (2009)
90. Mészáros P *High Energy Radiation from Magnetized Neutron Stars* (Chicago: Univ. of Chicago Press, 1992)
91. Beskin V S, Gurevich A V, Istomin Ya N *Physics of the Pulsar Magnetosphere* (Cambridge: Cambridge Univ. Press, 1993)
92. Craighead H G *Science* **290** 1532 (2000)
93. Opher M et al. *Phys. Plasmas* **8** 2454 (2001)
94. Shapiro S L, Teukolsky S A *Black Holes, White Dwarfs, and Neutron Stars*: *The Physics of Compact Objects* (Weinheim: Wiley-VCH, 2004)
95. Benvenuto O G, De Vito M A *Mon. Not. R. Astron. Soc.* **362** 891 (2005)
96. Chabrier G, Douchin F, Potekhin A Y *J. Phys. Condens. Matter* **14** 9133 (2002)
97. Chabrier G, Sauma D, Potekhin A Y *J. Phys. A Math. Gen.* **39** 4411 (2006)
98. Lai D *Rev. Mod. Phys.* **73** 629 (2001); Harding A K, Lai D *Rep. Prog. Phys.* **69** 2631 (2006)
99. Lau Y Y et al. *Phys. Rev. Lett.* **66** 1446 (1991)
100. Ang L K, Kwan T J T, Lau Y Y *Phys. Rev. Lett.* **91** 208303 (2003)
101. Ang L K, Lau Y Y, Kwan T J T *IEEE Trans. Plasma Sci.* **32** 410 (2004)
102. Ang L K et al. *Phys. Plasmas* **13** 056701 (2006)
103. Ang L K, Zhang P *Phys. Rev. Lett.* **98** 164802 (2007)
104. Shukla P K, Eliasson B *Phys. Rev. Lett.* **100** 036801 (2008)
105. Shpatakovskaya G V *Zh. Eksp. Teor. Fiz.* **129** 533 (2006) [*JETP* **102** 466 (2006)]
106. Barnes W L, Dereux A, Ebbesen T W *Nature* **424** 824 (2003)
107. Chang D E et al. *Phys. Rev. Lett.* **97** 053002 (2006)
108. Marklund M et al. *Europhys. Lett.* **84** 17006 (2008)
109. Markovich P A et al. *Semiconductor Equation* (Wien: Springer, 1990)
110. Abrahams E, Kravchenko S V, Sarachik M P *Rev. Mod. Phys.* **73** 251 (2001)
111. Magnus W C J, Schoenmaker W J *Quantum Transport in Submicron Devices* (Berlin: Springer, 2002)
112. Crouseilles N, Hervieux P-A, Manfredi G *Phys. Rev. B* **78** 155412 (2008)
113. Becker K H, Schoenbach K H, Eden J G *J. Phys. D* **39** R55 (2006)
114. Serbeto A et al. *Phys. Plasmas* **15** 013110 (2008)
115. Piovella N et al. *Phys. Rev. Lett.* **100** 044801 (2008)
116. Lindl J *Phys. Plasmas* **2** 3933 (1995)
117. Tabak M et al. *Phys. Plasmas* **1** 1626 (1994); **12** 057305 (2005)
118. Glenzer S H et al. *Phys. Rev. Lett.* **98** 065002 (2007)
119. Benney D J, Newell A C *J. Math. Phys.* (*MIT*) **46** 81 (1967)
120. Benjamin T B *Proc. R. Soc. London A* **299** 59 (1967)
121. Scott A C et al. *Proc. IEEE* **66** 1444 (1973)
122. Hasegawa A, Tappert F *Appl. Phys. Lett.* **23** 142, 171 (1973)
123. Agrawal G P *Nonlinear Fiber Optics* (Amsterdam: Elsevier/Academic Press, 2007)
124. Wan W, Jia S, Fleischer J W *Nature Phys.* **3** 46 (2007)
125. Karpman V I, Krushkal E M *Zh. Eksp. Teor. Fiz.* **55** 530 (1968) [*Sov. Phys. JETP* **28** 277 (1969)]
126. Karpman V I *Plasma Phys.* **13** 477 (1971)
127. Zakharov V E *Zh. Eksp. Teor. Fiz.* **62** 1745 (1972) [*Sov. Phys. JETP* **35** 908 (1972)]
128. Karpman V I *Nelineinye Volny v Dispergiruyushchikh Sredakh* (Nonlinear Waves in Dispersive Media) (Moscow: Nauka, 1973) [Translated into English (New York: Pergamon Press, 1975)]
129. Schamel H, Shukla P K *Phys. Rev. Lett.* **36** 968 (1976)
130. Shukla P K *Nature* **274** 874 (1978)
131. Sulem C, Sulem P-L *The Nonlinear Schrödinger Equation*: *Self-Focusing and Wave Collapse* (New York: Springer, 1999)
132. Fedele R *Phys. Scripta* **65** 502 (2002)

133. Dauxois T, Peyrard M *Physics of Solitons* (Cambridge: Cambridge Univ. Press, 2006)
134. Barenghi C F, Donnelly R J, Vinen W F (Eds) *Quantized Vortex Dynamics and Superfluid Turbulence* (Berlin: Springer, 2001)
135. Bewley G P, Lathrop D P, Sreenivasan K R *Nature* **441** 588 (2006)
136. Bose S N *Z. Phys.* **26** 178 (1924)
137. Einstein A *Sitzungsber. K. Preuß Akad. Wiss. Phys. Math. K1.* 261 (1924)
138. Gross E P *Nuovo Cimento* **20** 454 (1961)
139. Pitaevskii L P *Zh. Eksp. Teor. Fiz.* **40** 646 (1961) [*Sov. Phys. JETP* **13** 451 (1961)]
140. Pitaevskii L, Stringari S *Bose–Einstein Condensation* (Oxford: Clarendon Press, 2003)
141. Dalfovo F et al. *Rev. Mod. Phys.* **71** 463 (1999)
142. O'Dell D H J, Giovanazzi S, Eberlein C *Phys. Rev. Lett.* **92** 250401 (2004)
143. Pauli W *Z. Phys.* **32** 111 (1925); *Rev. Mod. Phys.* **13** 203 (1941)
144. Berestetskii V B, Lifshitz E M, Pitaevskii L P *Kvantovaya Elektrodinamika* (Quantum Electrodynamics) (Moscow: Nauka, 1980) [Translated into English (Oxford: Butterworth-Heinemann, 1999) p. 123]
145. Brodin G, Marklund M *New J. Phys.* **9** 277 (2007)
146. Dvornikov M, arXiv:0902.4596
147. Kolomeisky E B et al. *Phys. Rev. Lett.* **85** 1146 (2000)
148. Ivonin I A *Zh. Eksp. Teor. Fiz.* **112** 2252 (1997) [*JETP* **85** 1233 (1997)]
149. Ivonin I A, Pavlenko V P, Persson H *Phys. Rev. E* **60** 492 (1999)
150. Whitham G B *Linear and Nonlinear Waves* (New York: John Wiley & Sons, 1999)
151. Sagdeev R Z, in *Voprosy Teorii Plazmy* (Reviews of Plasma Physics) Vol. 4 (Ed. M A Leontovich) (Moscow: Atomizdat, 1964) p. 20 [Translated into English (New York: Consultants Bureau, 1966) p. 23]
152. Sagdeev R Z *Rev. Mod. Phys.* **51** 11 (1979)
153. Shukla P K, Yu M Y *J. Math. Phys.* **19** 2506 (1978); Yu M Y, Shukla P K, Bujarbarua S *Phys. Fluids* **23** 2146 (1980)
154. Gottlieb D, Orszag S A *Numerical Analysis of Spectral Methods: Theory and Applications* (Philadelphia: SIAM, 1977)
155. Kolmogorov A N *Dokl. Akad. Nauk SSSR* **30** 301 (1941); **31** 438 (1941) [*C.R.* (*Dokl.*) *Acad. Sci. USSR* **30** 301 (1941); **31** 438 (1941)]
156. Lesieur M *Turbulence in Fluids: Stochastic and Numerical Modelling* 2nd ed. (Dordrecht: Kluwer Acad. Publ., 1990)
157. Frisch U *Turbulence: the Legacy of A.N. Kolmogorov* (Cambridge: Cambridge Univ. Press, 1995)
158. Eyink G L, Sreenivasan K R *Rev. Mod. Phys.* **78** 87 (2006)
159. Iroshnikov P S *Astron. Zh.* **40** 742 (1963) [*Sov. Astron.* **7** 566 (1964)]
160. Kraichnan R H *Phys. Fluids* **8** 1385 (1965)
161. Larichev V D, McWilliams J C *Phys. Fluids A* **3** 938 (1991)
162. Scott R K *Phys. Rev. E* **75** 046301 (2007)
163. Paoletti M S et al. *Phys. Rev. Lett.* **101** 154501 (2008)
164. Eliasson B, Shukla P K *Phys. Rep.* **422** 225 (2006)
165. Haas F, Eliasson B, Shukla P K, Manfredi G *Phys. Rev. E* **78** 056407 (2008)
166. Kruer W L, Dawson J M, Sudan R N *Phys. Rev. Lett.* **23** 838 (1969)
167. Albrecht-Marc M et al. *Phys. Plasmas* **14** 072704 (2007)
168. Luque A, Schamel H, Fedele R *Phys. Lett. A* **324** 185 (2004)
169. Biermann L *Z. Naturforsch. A* **5** 65 (1950)
170. Weibel E S *Phys. Rev. Lett.* **2** 83 (1959)
171. Gruzinov A *Astrophys. J.* **563** L15 (2001)
172. Schlickeiser R, Shukla P K *Astrophys. J.* **599** L57 (2003)
173. Washimi H, Karpman V I *Zh. Eksp. Teor. Fiz.* **71** 1010 (1976) [*Sov. Phys. JETP* **44** 528 (1976)]
174. Karpman V I, Washimi H *J. Plasma Phys.* **18** 173 (1977)
175. Gradov O M, Stenflo L *Z. Naturforsch. A* **35** 461 (1980)
176. Gradov O M, Stenflo L *Phys. Lett. A* **95** 233 (1983)
177. Shukla P K, Yu M Y *Plasma Phys. Control. Fusion* **26** 841 (1984)
178. Shukla P K et al. *Phys. Rep.* **138** 1 (1986)
179. Tsintsadze L N, Shukla P K *Phys. Lett. A* **187** 67 (1994)
180. Tsintsadze L N, Shukla P K *J. Plasma Phys.* **74** 431 (2008)
181. Haas F *Phys. Plasmas* **15** 022104 (2008)
182. Haas F, Lazar M *Phys. Rev. E* **77** 046404 (2008)
183. Haas F, Shukla P K, Eliasson B *J. Plasma Phys.* **75** 251 (2009)
184. Pines D, Nozières P *The Theory of Quantum Liquids* (New York: W.A. Benjamin, 1966)
185. Lindhard J *Danske Vid. Selsk. Mat.-Fys. Medd.* **28** (8) 1 (1954)
186. Cockayne E, Levine Z H *Phys. Rev. B* **74** 235107 (2006)
187. Wei M S et al. *Phys. Rev. E* **70** 056412 (2004)
188. Estabrook K *Phys. Rev. Lett.* **41** 1808 (1978)
189. Abramowitz M, Stegun I A (Eds) *Handbook of Mathematical Functions with Formulas, Graphs, and Mathematical Tables* (New York: Dover Publ., 1972) [Translated into Russian (Moscow: Nauka, 1979)]
190. Lewin L *Polylogarithms and Associated Functions* (New York: North-Holland, 1981)
191. von Rooss O *Phys. Rev.* **119** 1174 (1960)
192. Arista N R, Brandt W *Phys. Rev. A* **29** 1471 (1984)
193. Leemans W P et al. *Phys. Rev. A* **46** 1091 (1992)
194. Fried B D, Conte S D *The Plasma Dispersion Function; the Hilbert Transform of the Gaussian* (New York: Academic Press, 1961)
195. Krall N A, Trivelpiece A W *Principles of Plasma Physics* (New York: McGraw-Hill, 1973)
196. Davidson R C et al. *Phys. Fluids* **15** 317 (1972)
197. Eliasson B *J. Comput. Phys.* **225** 1508 (2007)
198. Shukla P K, Shukla N, Stenflo L *J. Plasma Phys.* **75** (2009) (in press)
199. Oberman C, Ron A *Phys. Rev.* **130** 1291 (1963)
200. Kelley D C *Phys. Rev.* **134** A641 (1964)
201. Benford G, Rostoker N *Phys. Rev.* **181** 729 (1969)
202. Kuzelev M V, Rukhadze A A *Usp. Fiz. Nauk* **169** 687 (1999) [*Phys. Usp.* **42** 603 (1999)]
203. Melrose D B, Weise J I *Phys. Plasmas* **9** 4473 (2002)
204. Ginzburg V L *Raspredelenie Elektromagnitnykh Voln v Plazme* (Propagation of Electromagnetic Waves in Plasma) (Moscow: Fizmatgiz, 1960) [Translated into English (New York: Gordon and Breach, 1962)]
205. Abdullaev A Sh *Fiz. Plazmy* **14** 365 (1988) [*Sov. J. Plasma Phys.* **14** 214 (1988)]
206. Eliezer S et al. *Phys. Plasmas* **12** 052115 (2005)
207. Boosé D, Perez A *Phys. Lett. A* **234** 113 (1997)
208. Kittel C *Introduction to Solid State Physics* 7th ed. (New York: Wiley, 1996) Ch. 14 [Translated into Russian (Moscow: Nauka, 1978)]
209. Marklund M, Eliasson B, Shukla P K *Phys. Rev. E* **76** 067401 (2007)
210. Shaikh D, Shukla P K *Phys. Rev. Lett.* **102** 045004 (2009)
211. Drake J F et al. *Phys. Fluids* **17** 778 (1974)
212. Yu M Y, Spatschek K H, Shukla P K *Z. Naturforsch. A* **29** 1736 (1974)
213. Stenflo L *Phys. Scripta* **T30** 166 (1990)
214. Sagdeev R Z, Galeev A A *Nonlinear Plasma Theory* (New York: Benjamin, 1969)
215. Haas F *Phys. Plasmas* **14** 042309 (2007)
216. Haas F, Shukla P K *Phys. Rev. E* **79** 066402 (2009)
217. Marburger J H, Tooper R H *Phys. Rev. Lett.* **35** 1001 (1975)
218. Hakim R, Heyvaerts J *Phys. Rev. A* **18** 1250 (1978)
219. Shabad A Y *Tr. Fiz. Inst. Akad. Nauk SSSR* **192** 5 (1988) [Translated ito English: *Polarization of the Vacuum and a Quantum Relativistic Gas in an External Field* (Proc. Lebedev Phys. Inst., Ed. V L Ginzburg) (New York: Nova Sci, Pub. Inc, 1991)]
220. Lamata L et al. *Phys. Rev. Lett.* **98** 253005 (2007)